JCI The Journal of Clinical Investigation

Cul4A-DDB1–mediated monoubiquitination of phosphoglycerate dehydrogenase promotes colorectal cancer metastasis via increased S-adenosylmethionine

Yajuan Zhang, … , Dawei Li, Weiwei Yang

J Clin Invest. 2021;131(21):e146187. https://doi.org/10.1172/JCI146187.

Research Article | Metabolism | Oncology

Graphical abstract

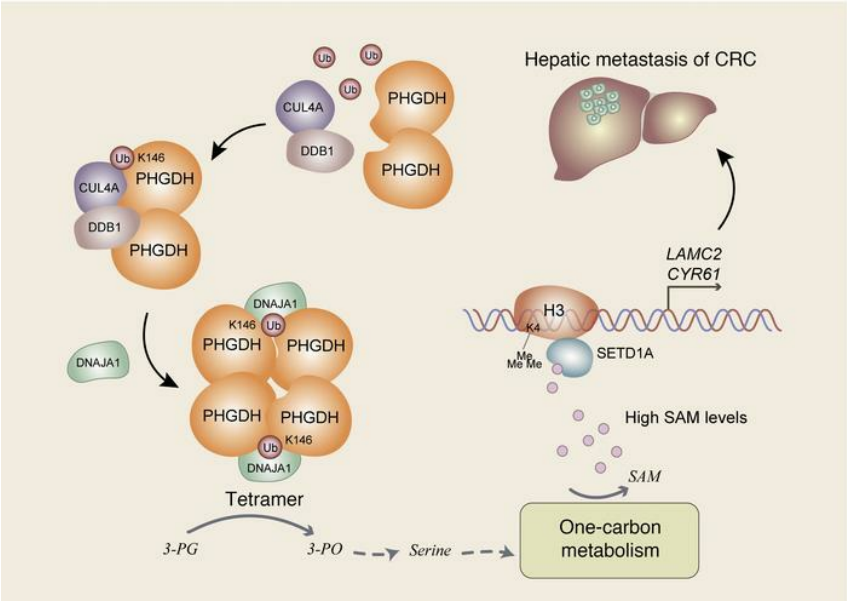

Find the latest version:

https://jci.me/146187/pdf

Cul4A-DDB1–mediated monoubiquitination of phosphoglycerate dehydrogenase promotes colorectal cancer metastasis via increased *S*-adenosylmethionine

Yajuan Zhang,[1] Hua Yu,[2] Jie Zhang,[3] Hong Gao,[1] Siyao Wang,[1] Shuxian Li,[3] Ping Wei,[4] Ji Liang,[1] Guanzhen Yu,[5] Xiongjun Wang,[2] Xinxiang Li,[6] Dawei Li,[6] and Weiwei Yang[1,7]

[1]State Key Laboratory of Cell Biology, Shanghai Key Laboratory of Molecular Andrology, Shanghai Institute of Biochemistry and Cell Biology, Center for Excellence in Molecular Cell Science, Chinese Academy of Sciences, University of Chinese Academy of Sciences, Shanghai, China. [2]Precise Genome Engineering Center, School of Life Sciences, Guangzhou University, Guangzhou, China. [3]School of Life Science and Technology, ShanghaiTech University, Shanghai, China. [4]Department of Pathology, Fudan University Shanghai Cancer Center, Shanghai, China. [5]Medical Artificial Intelligence Laboratory, Zhejiang Institute of Digital Media, Chinese Academy of Sciences, Shaoxing, China. [6]Department of Colorectal Surgery, Fudan University Shanghai Cancer Center, Shanghai, China. [7]School of Life Science, Hangzhou Institute for Advanced Study, University of Chinese Academy of Sciences, Hangzhou, China.

Although serine metabolism plays a crucial role in the proliferation and survival of tumor cells, how it supports tumor cell migration remains poorly understood. Phosphoglycerate dehydrogenase (PHGDH) catalyzes the oxidation of 3-phosphoglycerate to 3-phosphonooxypyruvate, the first committed step in de novo serine biosynthesis. Here we show that PHGDH was monoubiquitinated by cullin 4A–based E3 ligase complex at lysine 146 in colorectal cancer (CRC) cells, which enhanced PHGDH activity by recruiting a chaperone protein, DnaJ homolog subfamily A member 1, to promote its tetrameric formation, thereby increasing the levels of serine, glycine, and *S*-adenosylmethionine (SAM). Increased levels of SAM upregulated the expression of cell adhesion genes (laminin subunit gamma 2 and cysteine rich angiogenic inducer 61) by initiating SET domain containing 1A–mediated trimethylation of histone H3K4, thereby promoting tumor cell migration and CRC metastasis. Intriguingly, SAM levels in tumors or blood samples correlated with the metastatic recurrence of patients with CRC. Our finding not only reveals a potentially new role and mechanism of SAM-promoted tumor metastasis but also demonstrates a regulatory mechanism of PHGDH activity by monoubiquitination.

Introduction

Colorectal cancer (CRC) is the third most commonly diagnosed cancer in males and the second in females (1). Approximately 25% of patients with CRC are diagnosed with metastatic disease, and around 30% of cases that are diagnosed at earlier stages subsequently metastasize (2). Metastasis is a multistep, cascading process that is tightly regulated by a group of cell signaling proteins and continues to cause more than 90% of human cancer deaths. A study of the molecular mechanisms regulating metastasis assumes great significance for the treatment of patients with CRC.

Serine metabolism provides the essential precursors for the synthesis of proteins, nucleic acids, and lipids that are crucial to tumor cell growth. Moreover, serine biosynthesis affects cellular antioxidative capacity, thereby maintaining redox homeostasis in tumor cells (3). Imported serine and serine derived from glycolysis can be converted to glycine, which in turn provides carbon units for 1-carbon metabolism. One-carbon metabolism involving the folate and methionine cycles integrates nutritional status from amino acids, glucose, and vitamins and generates diverse outputs, such as the biosynthesis of lipids, nucleic acids, and proteins; the maintenance of redox status; and the substrates for methylation reactions (4). However, little is known about how serine metabolism contributes to tumor metastasis.

Phosphoglycerate dehydrogenase (PHGDH) is the key enzyme that catalyzes the first committed step of de novo serine biosynthesis. It diverts flux away from glycolysis by oxidizing 3-phosphoglycerate (3-PG) to release serine and glycine, thus allowing the rapid production of metabolites required for the high rate of anabolism. In recent years, the importance of PHGDH in cancer has been gradually recognized. Suppressing PHGDH activity causes a reduction in serine synthesis and subsequent strong decrease in breast cancer cell proliferation (5). Enhanced PHGDH activity by the loss of PKC-ζ in mice promotes intestinal tumorigenesis (6). In addition, hypoxia-induced enrichment of breast cancer stem cells requires PHGDH (7). However, the role and regulatory mechanism of PHGDH in CRC metastasis remain largely unknown.

In this study, we investigated the role and regulatory mechanism of PHGDH in CRC metastasis. We found that PHGDH is monoubiquitinated by cullin 4A–based (Cul4A-based) E3 ligase complex in CRC cells, which increases PHGDH activity and the levels of methyl donor *S*-adenosylmethionine (SAM), thereby upregulating cell adhesion gene expression via SET domain con-

Authorship note: YZ, HY, and JZ contributed equally to this work.
Conflict of interest: The authors have declared that no conflict of interest exists.

Submitted: December 7, 2020; **Accepted:** September 2, 2021;
Published: November 1, 2021.
Reference information: *J Clin Invest*. 2021;131(21):e146187.
https://doi.org/10.1172/JCI146187.

taining 1A–mediated (SETD1A-mediated) histone methylation to promote CRC metastasis.

Results

PHGDH expression correlates with CRC metastasis. To define the relationship between PHGDH and CRC, we analyzed the transcription of *PHGDH* in RNA-sequencing data of colon adenocarcinoma from The Cancer Genome Atlas (TCGA), showing that tumor tissues had much higher mRNA levels of PHGDH than normal tissues and that higher mRNA levels of PHGDH correlated with advanced tumor stages (Figure 1, A and B). Also, we compared overall survival duration of patients with CRC with PHGDH expression and found that higher levels of PHGDH correlated with worse patient prognosis in patients with CRC at advanced stages (III + IV) but not in patients with CRC at early stages (I + II) (Figure 1C and Supplemental Figure 1A). Of note, the levels of PHGDH had no correlation with patient prognosis in patients with CRC at all stages (I + II + III + IV) (Supplemental Figure 1B).

Moreover, we examined the protein levels of PHGDH in tumor tissues and paired peritumoral tissues from patients with CRC by performing IHC analyses with anti-PHGDH antibody, which showed that tumor tissues had much higher protein levels of PHGDH than the paired peritumoral tissues (Figure 1D). The specificity of anti-PHGDH antibody for IHC analysis was validated by recombinant PHGDH protein block assay (Supplemental Figure 1C) and IHC analysis of PHGDH protein in tumors from the mice implanted with HCT116 cells stably expressing nontargeting shRNA (shNT) or shPHGDH (Supplemental Figure 1D).

In addition, we compared PHGDH expression in the primary tumor tissues between patients with CRC with or without metastatic recurrences. IHC analysis with anti-PHGDH antibody showed that the tumors from patients with metastatic recurrences had much higher protein levels of PHGDH than the tumors from patients without metastatic recurrences (Figure 1E). Moreover, metastatic tumors dissected in the liver tissues from patients with CRC exhibited higher protein levels of PHGDH than the paired primary tumors from patients with CRC (Figure 1F). Taken together, these results suggest that PHGDH might play an important role in CRC metastasis.

PHGDH activity is essential for tumor cell migration and CRC metastasis. To determine the role of PHGDH in tumor cell migration, we depleted endogenous PHGDH in HCT116 or SW480 CRC cells with shRNA and rescued with shRNA-resistant (r) PHGDH WT or PHGDH enzymatic-dead (ED) mutant (PHGDH R236E; Supplemental Figure 1E). Transwell migration assay showed that PHGDH depletion greatly inhibited tumor cell migration, and reexpressing rPHGDH WT fully recovered PHGDH depletion–inhibited tumor cell migration, excluding the possibility of off-target effect of PHGDH shRNA. However, tumor cells reexpressing rPHGDH ED had much less migration than the cells reexpressing rPHGDH WT (Figure 1G and Supplemental Figure 1F), indicating that PHGDH activity was essential for tumor cell migration. Notably, PHGDH depletion did not affect HCT116 proliferation within 24 hours, during which Transwell migration assay was performed (Supplemental Figure 1G).

We further investigated the role of PHGDH activity in CRC metastasis by using a mouse model of hepatic metastasis via intraspleen injection, which showed that PHGDH depletion greatly inhibited tumor metastasis, while rescued expression of rPHGDH WT, but not that of rPHGDH ED, restored hepatic metastasis of PHGDH-depleted tumor cells (Figure 1H and Supplemental Figure 1H). The hepatic nodules were dissected and validated to be metastatic tumors by H&E staining (Supplemental Figure 1I). These results support that PHGDH activity is required for CRC metastasis.

In addition, we established a patient-derived xenograft (PDX) model of CRC metastasis and treated these tumor-bearing mice with or without PHGDH inhibitor (NCT-503). The administration of NCT-503 dramatically inhibited hepatic metastasis of CRC cells (Figure 1I and Supplemental Figure 1, J and K). Notably, NCT-503 treatment also inhibited the growth of primary tumors (Supplemental Figure 1L). The efficacy of NCT-503 was validated by PHGDH activity assay, which showed that NCT-503–treated PDX tumors had much lower PHGDH activity than control PDX tumors (Supplemental Figure 1M). However, Transwell migration assay within 24 hours showed that NCT-503 treatment greatly inhibited tumor cell migration (Figure 1J). Within 24 hours, NCT-503 treatment had no significant influence on tumor cell proliferation (Supplemental Figure 1N). Collectively, these results indicate that the inhibition of both cell proliferation and cell migration contributes to the impairment of tumor metastasis by NCT-503.

Monoubiquitination increases PHGDH activity through DnaJ homolog subfamily A member 1–dependent PHGDH tetrameric formation. The activity of metabolic enzymes is commonly regulated by posttranslational modifications, such as phosphorylation, acetylation, or ubiquitination. As indicated in PhosphoSitePlus database (https://www.phosphosite.org/homeAction.action), PHGDH is extensively ubiquitinated. Thus, we wondered whether PHGDH was ubiquitinated. To determine PHGDH's ubiquitination, we generated HCT116 or SW480 cells stably overexpressing S-Flag-Streptavidin-binding peptide–tagged (SFB-tagged) PHGDH (SFB-PHGDH) and HA-tagged ubiquitin (HA-Ub). Intriguingly, immunoblotting analysis of immunoprecipitated SFB-PHGDH with anti-HA antibody showed that PHGDH was monoubiquitinated (Figure 2A). This monoubiquitination was also detected in endogenous PHGDH in HCT116 and SW480 cells (Supplemental Figure 2A). Moreover, we analyzed the clinical relevance of PHGDH monoubiquitination by using co-IP assay with anti-PHGDH antibody in primary tumor tissues from patients with CRC with or without metastatic recurrence. Immunoblotting analysis of immunoprecipitated PHGDH with anti-ubiquitin antibody indicated that the patients with metastatic recurrence had much more monoubiquitination in PHGDH than those without metastatic recurrence (Supplemental Figure 2B).

To identify the ubiquitinated residues, we performed mass spectrometry analysis with SFB-PHGDH precipitated from HCT116 and observed that lysines (K) 21, K33, K69, K129, and K146 in PHGDH were potentially ubiquitinated (Supplemental Figure 2, C and D). We mutated these 5 ubiquitinated lysine residues into arginine (R), individually. As shown in Figure 2B, K146R among the mutations dramatically inhibited PHGDH monoubiquitination, while K21R slightly attenuated that, suggesting that K146 is the major monoubiquitinated residue. Additionally, we constructed PHGDH K21/146R mutant and found that PHGDH

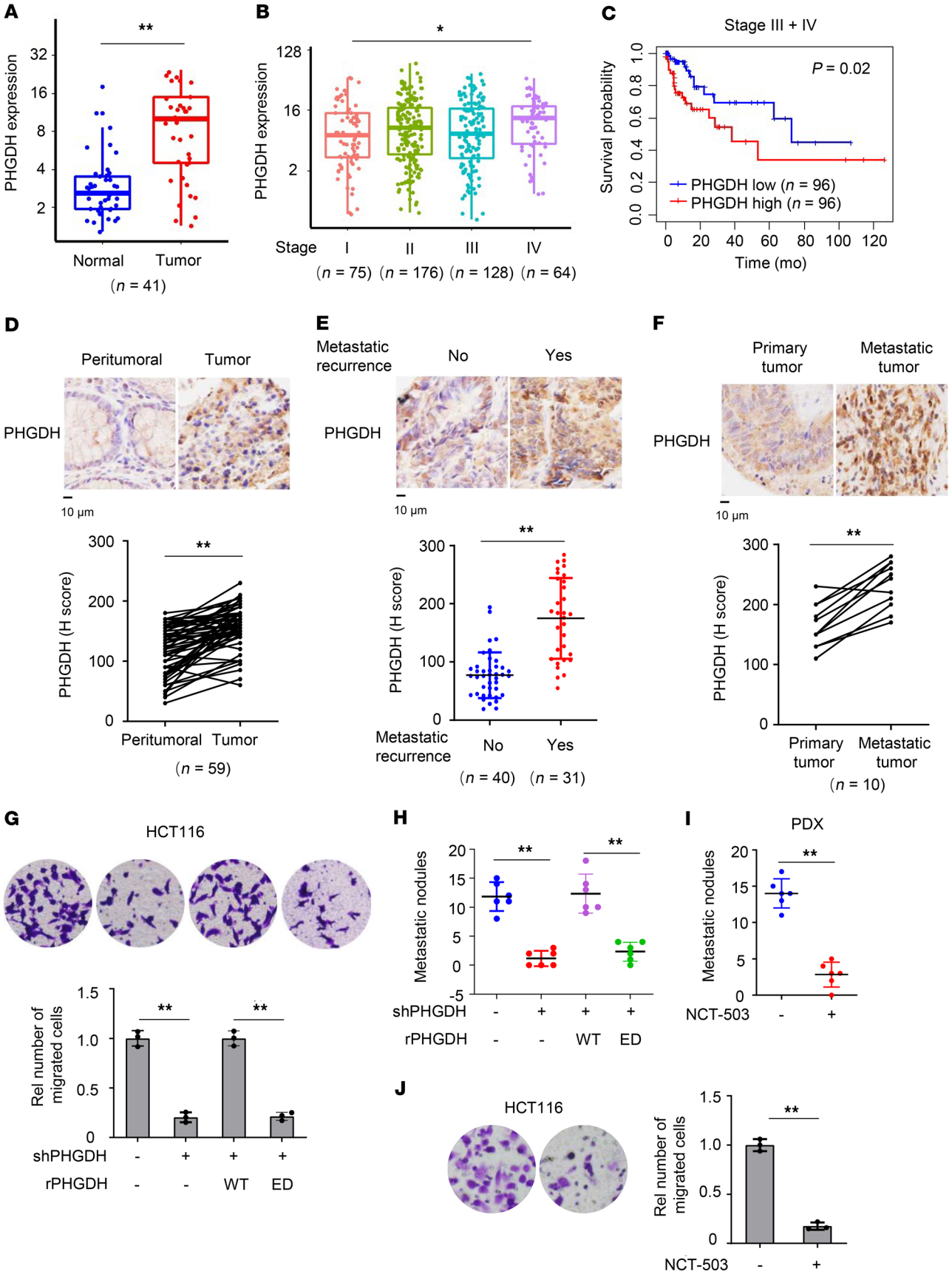
A
B
C
Stage III + IV
P = 0.02
PHGDH low (n = 96)
PHGDH high (n = 96)
Survival probability
Time (mo)
PHGDH expression
Normal
Tumor
(n = 41)
Stage
(n = 75) (n = 176) (n = 128) (n = 64)
D
E
F
Peritumoral
Tumor
PHGDH
10 μm
PHGDH (H score)
(n = 59)
Metastatic recurrence
No
Yes
(n = 40) (n = 31)
Primary tumor
Metastatic tumor
(n = 10)
G
HCT116
Rel number of migrated cells
shPHGDH
rPHGDH
WT
ED
H
Metastatic nodules
I
PDX
NCT-503
J

Figure 1. PHGDH activity is important for CRC metastasis. (**A**–**C**) TCGA RNA-sequencing data of patients with colon adenocarcinoma were analyzed. *PHGDH* mRNA levels were compared between tumors and paired normal tissues (**A**) or between different stages (**B**) (Wilcoxon's signed-rank test). The boxes represent the median and the first and third quartiles, and the whiskers represent the minimum and maximum of all data points. Survival durations of 192 patients with low or high expression of *PHGDH* were compared (Kaplan-Meier method, **C**). (**D**–**F**) IHC analyses of PHGDH were performed in tumors and paired peritumoral tissues (**D**), primary tumors with or without metastatic recurrence (**E**), or paired primary tumors and metastatic tumors in the livers (**F**) from patients with CRC. Top, representative IHC staining images. Bottom, semiquantitative scoring (H score). **D** and **F**, paired *t* test, 2 tailed. **E**, Data represent mean ± SD (2-tailed *t* test). (**G** and **H**) HCT116 cells stably expressing shNT or PHGDH were infected with the lentivirus expressing rPHGDH WT or ED. Transwell migration assays were performed (**G**). Representative images (top) and statistical analyses (bottom) of the migrated cells were shown. Data represent mean ± SD of 3 biologically independent experiments. The cells were injected into spleens of randomized BALB/c nude mice. The metastatic nodules in the livers were counted and statistically analyzed (**H**). Data represent mean ± SD of 6 mice. One-way ANOVA with Tukey's multiple-comparison test. Rel, relative. (**I**) Metastatic tumors were dissected from patients with CRC with hepatic metastasis and subcutaneously implanted into randomized BALB/c nude mice. Mice were treated with or without NCT-503. Metastatic nodules in the livers were counted and statistically analyzed. Data represent the mean ± SD of 6 mice (2-tailed *t* test). (**J**) Transwell migration assays were performed in HCT116 cells treated with or without 10 μM NCT-503. Data represent the mean ± SD of 3 biologically independent experiments (2-tailed *t* test). $^{*}P < 0.05$, $^{**}P < 0.01$. See also Supplemental Figure 1.

monoubiquitination was almost completely abolished by K21/146R mutation (Supplemental Figure 2E).

We next examined whether K146 monoubiquitination (K146mUb) influenced PHGDH activity. PHGDH K146R had much lower activity than PHGDH WT (Figure 2C). In contrast, PHGDH K21R mutation did not affect PHGDH activity (Supplemental Figure 2F). PHGDH is the key metabolic enzyme of serine and glycine biosynthesis. Serine and glycine provide carbon units for 1-carbon metabolism. SAM, which is generated via 1-carbon metabolism, is the main methyl donor in methylation reactions (8). We thus measured the levels of those PHGDH-regulated downstream metabolites, including serine, glycine, and SAM, which showed that PHGDH-depleted HCT116 and SW480 cells rescued with rPHGDH K146R had much lower levels of serine, glycine, and SAM than the cells rescued with rPHGDH WT (Figure 2D and Supplemental Figure 2G). Of note, PHGDH K146R mutation did not affect PHGDH expression (Supplemental Figure 2H). Moreover, we subcutaneously implanted PHGDH-depleted HCT116 cells rescued with rPHGDH WT or K146R into BALB/c nude mice and found that the tumors harboring rPHGDH K146R had lower SAM levels than the tumors harboring rPHGDH WT (Figure 2E). These results demonstrate that K146mUb enhances the enzymatic activity of PHGDH.

Additionally, to demonstrate that altered levels of serine, glycine, and SAM result from altered activity of PHGDH and the serine biosynthesis pathway, we depleted phosphoserine aminotransferase (PSAT1), another enzyme in the pathway, in PHGDH-depleted HCT116 cells rescued with rPHGDH WT or K146R. PSAT1 depletion, similar to rPHGDH K146R expression, also greatly decreased the levels of serine, glycine, and SAM in the cells. In the presence of PSAT1 depletion, rPHGDH K146R expression could not further decrease the levels of serine, glycine, and SAM in the cells (Supplemental Figure 2, I and J). This result further supports that the PHGDH-regulated serine biosynthesis pathway is indeed essential for the levels of serine, glycine, and SAM in CRC cells.

To determine how monoubiquitination regulates PHGDH activity, we analyzed the structure of truncated human PHGDH (4–315 residues) (Protein Data Bank: 2G76) and found that K146 was located in the dimeric interface of PHGDH (Supplemental Figure 2K). Thus, we examined whether K146mUb affected PHGDH oligomerization. Gel filtration chromatography analysis of SFB-PHGDH WT or K146R precipitated from HCT116 cells showed that PHGDH K146R had many fewer tetrameric forms but more dimeric forms than PHGDH WT (Figure 2F), suggesting that PHGDH mainly exists as a tetramer in CRC cells and that K146mUb is required for its tetrameric formation. Notably, such tetrameric form was also observed in full-length PHGDH proteins from both *E. coli* and rat, which are composed of 4 identical, asymmetric subunits. Importantly, PHGDH activity is closely related to the tetrameric conformation (9, 10).

To investigate how K146mUb regulates PHGDH tetrameric formation, we analyzed mass spectrometry data of PHGDH-associated proteins and found a molecular chaperone, DnaJ homolog subfamily A member 1 (DNAJA1), ranked in the top 9 proteins with strong interaction with PHGDH (Supplemental Figure 2L). DNAJA1 is a member of the DNAJ family, which is involved in diverse cellular activities, including protein translation, folding/unfolding/refolding, translocation, and degradation (11). We confirmed the interaction of DNAJA1 and PHGDH by co-IP assay and further observed that PHGDH K146R had much less interaction with DNAJA1 than PHGDH WT (Figure 2G). To determine whether DNAJA1 is required for the tetrameric formation of PHGDH, we depleted DNAJA1 in HCT116 cells and rescued these cells with rDNAJA1 (Supplemental Figure 2M). Gel filtration chromatography analysis showed that DNAJA1 depletion decreased the percentage of tetrameric PHGDH, while rescued rDNAJA1 expression restored its tetrameric formation (Figure 2H). Consistently, DNAJA1 depletion greatly inhibited PHGDH activity, and rescued rDNAJA1 expression restored PHGDH activity (Figure 2I). In contrast, depletion of HSP70, another molecular chaperone identified in the mass spectrometry data of PHGDH-associated proteins, shown in Supplemental Figure 2L, did not affect PHGDH activity (Supplemental Figure 2, N and O).

Collectively, these results suggest that K146mUb recruits DNAJA1 to facilitate the tetrameric formation of PHGDH, thereby enhancing PHGDH activity.

Cul4A–DNA damage-binding protein 1–CUL4-associated factor 16 complex mediates the monoubiquitination of PHGDH. To identify the E3 ubiquitin ligase responsible for PHGDH K146mUb, we performed mass spectrometry analysis of PHGDH-associated proteins and observed that Cul4A, the core component of multiple cullin-RING–based E3 ubiquitin–protein ligase complexes that mediate the ubiquitination of target proteins, and DNA damage-binding protein 1 (DDB1) had strong interactions with PHGDH (Figure 3A). DDB1 is also a component of numerous distinct DDB1-CUL4–X-box (DCX) E3 ubiquitin–protein ligase

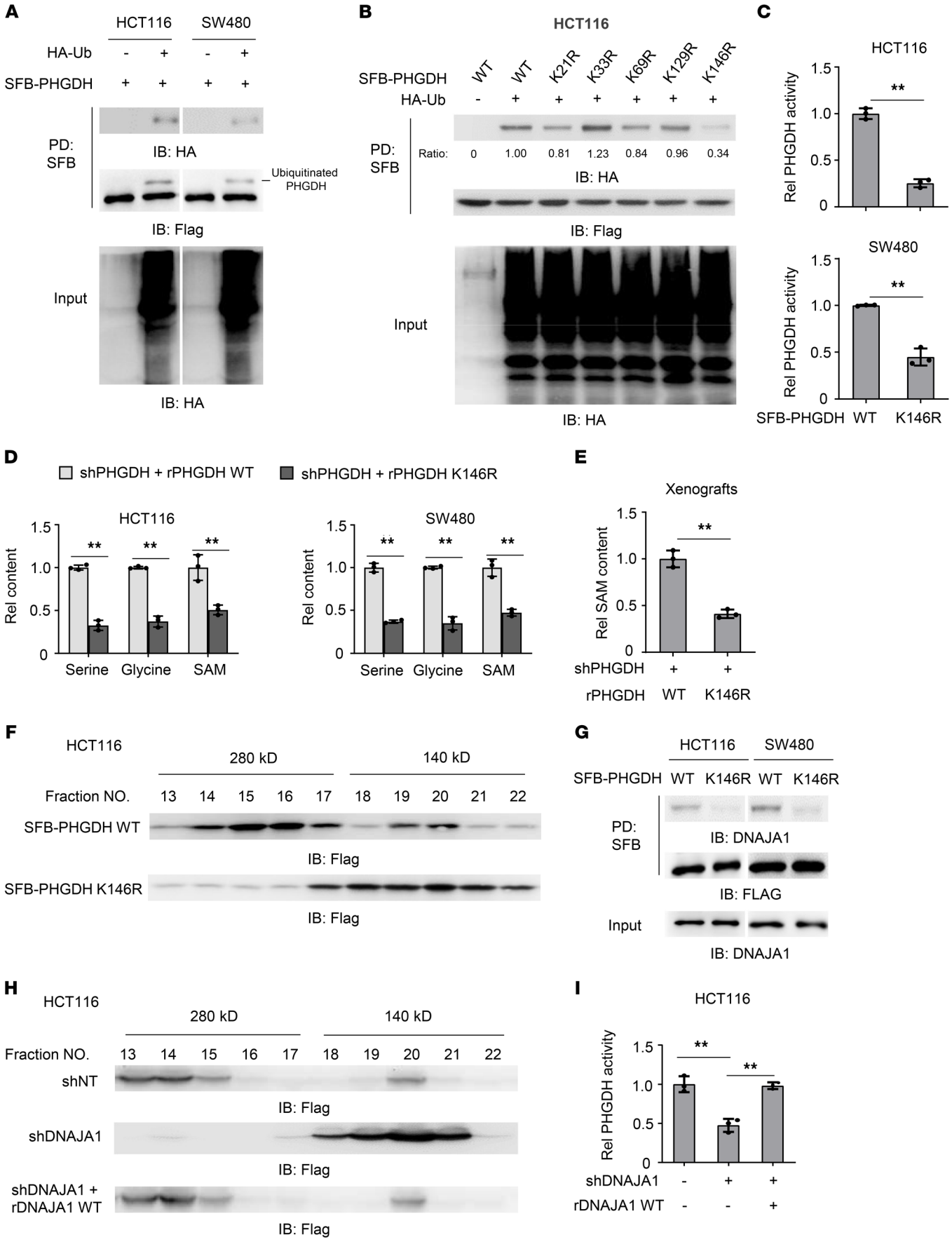
A
HCT116
SW480
HA-Ub
SFB-PHGDH
PD: SFB
IB: HA
Ubiquitinated PHGDH
IB: Flag
Input
IB: HA
B
HCT116
SFB-PHGDH
WT
K21R
K33R
K69R
K129R
K146R
HA-Ub
PD: SFB
Ratio: 0 1.00 0.81 1.23 0.84 0.96 0.34
IB: HA
IB: Flag
Input
IB: HA
C
HCT116
SW480
Rel PHGDH activity
SFB-PHGDH WT K146R
D
shPHGDH + rPHGDH WT
shPHGDH + rPHGDH K146R
HCT116
SW480
Rel content
Serine Glycine SAM
E
Xenografts
Rel SAM content
shPHGDH
rPHGDH WT K146R
F
HCT116
280 kD
140 kD
Fraction NO. 13 14 15 16 17 18 19 20 21 22
SFB-PHGDH WT
IB: Flag
SFB-PHGDH K146R
IB: Flag
G
HCT116
SW480
SFB-PHGDH WT K146R WT K146R
PD: SFB
IB: DNAJA1
IB: FLAG
Input
IB: DNAJA1
H
HCT116
280 kD
140 kD
Fraction NO. 13 14 15 16 17 18 19 20 21 22
shNT
IB: Flag
shDNAJA1
IB: Flag
shDNAJA1 + rDNAJA1 WT
IB: Flag
I
HCT116
Rel PHGDH activity
shDNAJA1
rDNAJA1 WT

Figure 2. Monoubiquitination increases PHGDH activity through DNAJA1-dependent PHGDH tetrameric formation. (**A**) HCT116 or SW480 cells stably overexpressing SFB-PHGDH were infected with the lentivirus expressing empty vector (EV) or HA-Ub. SFB-PHGDH proteins were pulled down with streptavidin agarose beads. PD, pulldown. (**B**) HCT116 cells stably expressing SFB-PHGDH WT or indicated mutants were transfected with or without HA-Ub. (**C**) SFB-PHGDH proteins were pulled down from HCT116 or SW480 cells stably expressing SFB-PHGDH WT or K146R using streptavidin agarose beads for PHGDH activity measurement. Two-tailed Student's *t* test. (**D**) PHGDH-depleted HCT116 or SW480 cells rescued with rPHGDH WT or K146R were harvested for the measurement of intracellular serine, glycine, and SAM. Two-tailed Student's *t* test. (**E**) PHGDH-depleted HCT116 cells rescued with rPHGDH WT or K146R were subcutaneously implanted into BALB/c nude mice. SAM levels in dissected tumors were measured. Data represent the mean ± SD of 3 mice (2-tailed Student's *t* test). (**F**) SFB-PHGDH proteins were pulled down from HCT116 cells stably expressing SFB-PHGDH WT or K146R for gel filtration chromatography analysis. (**G**) HCT116 or SW480 cells were infected with the lentivirus expressing SFB-PHGDH WT or K146R. SFB-PHGDH proteins were pulled down with streptavidin agarose beads. (**H** and **I**) HCT116 cells stably expressing SFB-PHGDH and shNT or shDNAJA1 were infected with the lentivirus expressing EV or rDNAJA1 WT. SFB-PHGDH proteins were pulled down for gel filtration chromatography analysis (**H**) and PHGDH activity measurement (**I**). (**I**) One-way ANOVA with Tukey's multiple-comparison test. (**C**, **D**, and **I**) Data represent the mean ± SD of 3 biologically independent experiments. $^{**}P < 0.01$. See also Supplemental Figure 2.

complexes. The functional specificity of the DCX E3 ligase complex is determined by the variable substrate recognition component recruited by DDB1. The interaction between Cul4A, DDB1, and PHGDH was further supported by co-IP assay with anti-PHGDH antibody (Figure 3B). Importantly, PHGDH K146mUb was increased by Cul4A overexpression, whereas K146R mutation abrogated such increased ubiquitination (Figure 3C). In contrast, depleting either Cul4A or DDB1 markedly decreased the monoubiquitination of PHGDH (Figure 3D).

The Cul4-DDB1–based E3 ligase binds to the target substrate through CUL4-associated factors (DCAFs), which act as substrate receptors. To identify the specific DCAFs targeting PHGDH, we reanalyzed our mass spectrometry data of PHGDH-associated proteins and noticed that DCAF16 was associated with PHGDH. The interaction between PHGDH and DCAF16 was validated by co-IP experiment (Supplemental Figure 3A). We thus depleted DCAF16 in HCT116 cells and found that DCAF16 depletion indeed dramatically attenuated PHGDH monoubiquitination (Supplemental Figure 3B). To further support that PHGDH monoubiquitination is mediated by Cul4A-DDB1-DCAF16 complex, we performed an in vitro ubiquitination assay by mixing Flag-Cul4A and HA-DCAF16, which were immunoprecipitated and purified from HEK293T cells stably expressing Flag-Cul4A or HA-DCAF16, with recombinant GST-PHGDH, His-ubiquitin (Ub), His-Uba1 (E1), and His-UbcH6 (E2). The result indicated that PHGDH was indeed monoubiquitinated in the presence of Cul4A-based E3 ligase complex (Figure 3E).

We next examined the activity of PHGDH in CRC cells with or without Cul4A or DDB1 depletion, which showed that the depletion of either Cul4A or DDB1 markedly decreased PHGDH activity (Figure 3F). Similarly, depleting Cul4A and DDB1 disrupted the interaction between PHGDH and DNAJA1 and dramatically decreased the levels of serine, glycine, and SAM (Figure 3G and Supplemental Figure 3C). Collectively, these results demonstrate that the monoubiquitination of PHGDH K146 is mediated by Cul4A-DDB1-DCAF16 complex, which regulates the enzymatic activity of PHGDH.

In addition, we compared Cul4A or DDB1 expression between paired metastatic tumors dissected in the liver tissues and primary tumors from patients with CRC. IHC analysis showed that higher Cul4A protein levels, but similar DDB1 protein levels, were observed in metastatic tumors, compared with the paired primary tumors (Figure 3H and Supplemental Figure 3D).

Increased SAM levels by PHGDH K146mUb promote CRC metastasis. To investigate the role of PHGDH K146mUb in tumor cell migration, we performed Transwell migration assay with PHGDH-depleted HCT116 and SW480 cells rescued with rPHGDH WT or K146R, which showed that rescued expression of rPHGDH K146R dramatically inhibited tumor cell migration. Importantly, supplementation of exogenous SAM completely restored SAM levels in tumor cells rescued with rPHGDH K146R and therefore greatly recovered the migration of these cells (Figure 4, A and B). Of note, tumor cells rescued with rPHGDH K146R had a similar proliferation rate to tumor cells rescued with rPHGDH WT (Supplemental Figure 4A).

Given that there are many metabolites downstream of PHGDH, we wondered whether other downstream metabolites, whose levels are regulated by PHGDH K146mUb, could rescue the migration of tumor cells expressing rPHGDH K146R. To test the hypothesis, we performed targeted metabolic profiling of the metabolites downstream of PHGDH, including serine and glycine biosynthesis pathway and 1-carbon metabolism pathway, in PHGDH-depleted HCT116 cells rescued with rPHGDH WT or K146R. The data showed that rescued expression of rPHGDH K146R did alter the levels of a series of metabolites, including serine, glycine, 5-methyl-tetrahydrofolate (5-m-THF), methionine, SAM, and *S*-adenosylhomocysteine (SAH) (Supplemental Figure 4B). Of note, not all the metabolites in the pathway were detected because of the technical limits. Serine, glycine, 5-m-THF, and methionine are the upstream precursors for SAM in the pathway and influence the levels of SAM. Therefore, we supplemented tumor cells rescued with rPHGDH K146R with SAH, the downstream metabolite of SAM. As shown in Supplemental Figure 4C, SAH supplementation did not rescue the migration of tumor cells rescued with rPHGDH K146R.

To confirm the role of PHGDH K146mUb in CRC metastasis, we implanted PHGDH-depleted HCT116 cells rescued with rPHGDH WT or K146R into randomized BALB/c nude mice via intraspleen injection. Rescued expression of rPHGDH K146R dramatically impaired the hepatic metastasis of CRC cells (Figure 4C and Supplemental Figure 4, D and E) and greatly extended the survival duration of the tumor-bearing mice (Figure 4D). Moreover, we orthotopically implanted luciferase-expressing PHGDH-depleted HCT116 cells rescued with rPHGDH WT or K146R into randomized nude mice. Bioluminescence imaging of dissected liver tissues confirmed that rescued expression of rPHGDH K146R dramatically impaired the hepatic metastasis of CRC cells (Figure 4E and Supplemental Figure 4F). Taken together, these results demonstrate that PHGDH K146mUb is essential for tumor cell migration and CRC metastasis.

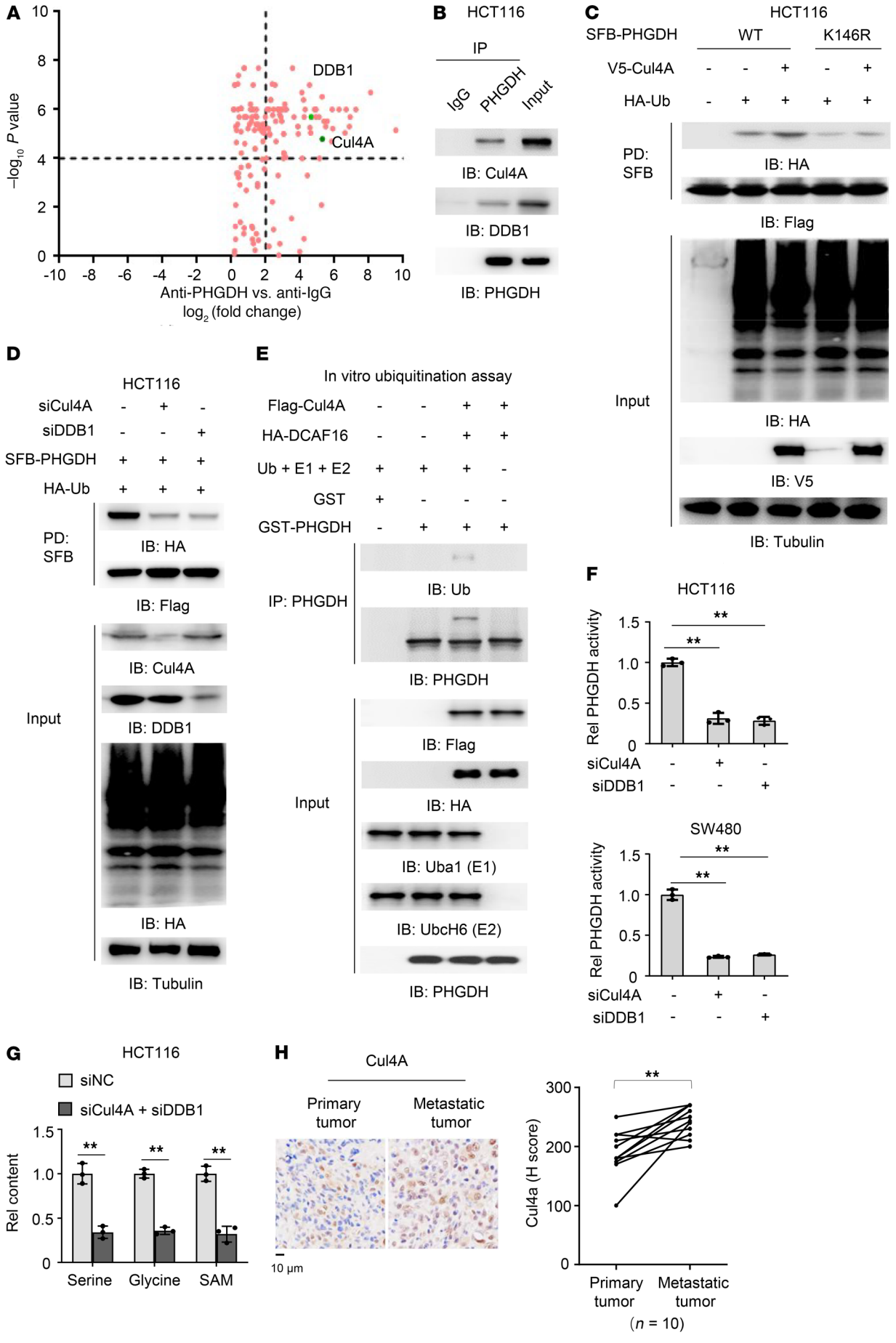
A
DDB1
Cul4A
−log10 P value
Anti-PHGDH vs. anti-IgG
log2 (fold change)
B
HCT116
IP
IgG
PHGDH
Input
IB: Cul4A
IB: DDB1
IB: PHGDH
C
HCT116
SFB-PHGDH
WT
K146R
V5-Cul4A
HA-Ub
PD: SFB
IB: HA
IB: Flag
Input
IB: V5
IB: Tubulin
D
HCT116
siCul4A
siDDB1
SFB-PHGDH
HA-Ub
PD: SFB
IB: HA
IB: Flag
IB: Cul4A
IB: DDB1
Input
IB: HA
IB: Tubulin
E
In vitro ubiquitination assay
Flag-Cul4A
HA-DCAF16
Ub + E1 + E2
GST
GST-PHGDH
IP: PHGDH
IB: Ub
IB: PHGDH
IB: Flag
IB: HA
Input
IB: Uba1 (E1)
IB: UbcH6 (E2)
IB: PHGDH
F
HCT116
Rel PHGDH activity
siCul4A
siDDB1
SW480
Rel PHGDH activity
siCul4A
siDDB1
G
HCT116
siNC
siCul4A + siDDB1
Rel content
Serine
Glycine
SAM
H
Cul4A
Primary tumor
Metastatic tumor
10 μm
Cul4a (H score)
Primary tumor
Metastatic tumor
(n = 10)

Figure 3. Cul4A–DDB1–CUL4-associated factor 16 complex mediates the monoubiquitination of PHGDH. (**A**) PHGDH proteins were immunoprecipitated from HCT116 cells and the immunoprecipitated complex was further analyzed by liquid chromatography–tandem mass spectrometry for identification of PHGDH-associated proteins. Data represent the means ± SD of 2 independent experiments. (**B**) HCT116 cells were harvested and PHGDH proteins were immunoprecipitated. (**C**) HCT116 cells stably expressing SFB-PHGDH WT or K146R were cotransfected with EV or HA-Ub and EV or V5-Cul4A. SFB-PHGDH proteins were pulled down using streptavidin agarose beads. (**D**) HCT116 cells stably expressing SFB-PHGDH were cotransfected with HA-Ub and siNC, siCul4A, or siDDB1. SFB-PHGDH proteins were pulled down using streptavidin agarose beads. (**E**) Flag-Cul4A and HA-DCAF16 were immunoprecipitated and purified from HEK293T cells stably expressing Flag-Cul4A or HA-DCAF16. In vitro ubiquitination assay was performed by incubating Flag-Cul4A and HA-DCAF16 with recombinant GST-PHGDH, His-ubiquitin (Ub), His-Uba1 (E1), and His-UbcH6 (E2). (**F**) HCT116 or SW480 cells stably expressing SFB-PHGDH were transfected with siNC, siCul4A, or siDDB1. SFB-PHGDH proteins were pulled down using streptavidin agarose beads for PHGDH activity measurement. One-way ANOVA with Tukey's multiple-comparison test. (**G**) HCT116 cells were transfected with siNC or siCul4A and siDDB1. Cells were harvested for the measurement of intracellular glycine, serine, and SAM (2-tailed Student's *t* test). (**F** and **G**) Data represent the mean ± SD of 3 biologically independent experiments. (**H**) IHC staining was performed in paired primary tumors and hepatic metastatic tumors from 10 patients with CRC with anti-Cul4A antibody. Staining scores of Cul4A were compared between primary tumors and metastatic tumors. Left, representative images of IHC staining were shown. Right, semiquantitative scoring was carried out (paired *t* test, 2 tailed). $^{**}P < 0.01$. See also Supplemental Figure 3.

Next, we wondered whether increased SAM levels sufficiently promote tumor cell migration. To test the hypothesis, we incubated HCT116 cells with increasing amounts of SAM and found that SAM promoted tumor cell migration in a dose-dependent manner (Figure 4F and Supplemental Figure 4G). Moreover, the administration of SAM via oral gavage greatly enhanced the hepatic metastasis of HCT116 cells in the mouse model of metastasis either via intraspleen injection or via orthotopic injection (Figure 4, G and H; and Supplemental Figure 4, H–J).

In addition, we examined SAM levels in metastatic tumors and paired primary tumors of patients with CRC and found that metastatic tumors had much higher SAM levels than the primary tumors (Figure 4I). Moreover, the patients with metastatic recurrence had much higher levels of SAM in blood samples than the patients without metastatic recurrence (Figure 4J), suggesting the diagnostic potential of blood SAM levels for CRC metastasis.

PHGDH monoubiquitination upregulates cell adhesion gene expression and promotes tumor cell migration. To determine the mechanism underlying PHGDH K146mUb–promoted tumor cell migration, we performed RNA-sequencing analysis for HCT116 cells with or without PHGDH depletion. Gene Ontology (GO) enrichment analysis indicated that cell motility and migration-related genes were the top 2 categories with significant alterations (Figure 5A). Among these genes, laminin subunit gamma 2 (*LAMC2*) and cysteine rich angiogenic inducer 61 (*CYR61*) have been well established to promote tumor cell migration (12, 13). We examined their expressions in PHGDH-depleted HCT116 or SW480 cells rescued with rPHGDH WT or K146R. Rescued expression of rPHGDH K146R dramatically decreased *LAMC2* and *CYR61* expressions, while SAM supplementation greatly restored their expressions in the cells rescued with rPHGDH K146R (Figure 5, B and C, and Supplemental Figure 5A). Also, knockdown of Cul4A and DDB1 inhibited *LAMC2* and *CYR61* expression (Supplemental Figure 5B). Moreover, we examined the expressions of these 2 genes in PDX tumors treated with or without NCT-503 and found that the inhibition of PHGDH activity markedly decreased *LAMC2* and *CYR61* expressions (Supplemental Figure 5C).

Among all the epigenetic features, trimethylation of histone H3K4 (H3K4me3) has been widely recognized as an active promoter mark. It was reported that over 80% of genes with promoter H3K4me3 were transcribed (14). To demonstrate how PHGDH K146mUb regulates the expressions of *LAMC2* and *CYR61*, we examined H3K4me3 at their promoters. Chromatin immunoprecipitation PCR (ChIP-PCR) assay showed that tumor cells rescued with rPHGDH K146R had much less H3K4me3 at their promoters than the cells rescued with rPHGDH WT (Figure 5D). Moreover, compared with histone H3 WT overexpression, the overexpression of histone H3K4R mutant, in which K4 was mutated to R, dramatically inhibited H3K4me3 and *LAMC2* and *CYR61* expression (Supplemental Figure 5, D and E). Of note, there was no significant difference in histone H3K9 acetylation (H3K9ac) at these 2 genes between PHGDH-depleted HCT116 cells rescued with rPHGDH WT or K146R, as determined by ChIP-PCR analysis (Supplemental Figure 5F). Taken together, these results demonstrate that PHGDH K146 monoubiquitination increases the expressions of cell adhesion genes *LAMC2* and *CYR61*, by regulating H3K4me3.

To test whether PHGDH K146mUb promotes tumor cell migration by upregulating *LAMC2* and *CYR61*, we overexpressed LAMC2 and CYR61 in PHGDH-depleted HCT116 cells rescued with rPHGDH K146R (Supplemental Figure 5G) and found that their overexpression completely recovered the migration of tumor cells rescued with rPHGDH K146R (Figure 5E). Notably, depletion of LAMC2 and CYR61 greatly inhibited hepatic metastasis of HCT116 cells (Supplemental Figure 5, H and I). These results suggest that PHGDH K146 monoubiquitination promotes tumor cell migration by upregulating the expressions of *LAMC2* and *CYR61*.

In addition, we examined the influence of SAM supplementation on histone methylation and the expression of *LAMC2* and *CYR61*, which showed that the supplementation of a high dose of SAM markedly increased H3K4me3 and the expression of these 2 genes (Figure 5, F and G).

Increased SAM levels by PHGDH K146mUb promote tumor cell migration by initiating SETD1A-mediated histone methylation of LAMC2 and CYR61. Six histone methyltransferases (HMTs), including KMT2A, KMT2C, KMT2D, SETD1A, SETD1B, and SMYD3, were reported to catalyze H3K4me3 under various circumstances (15). To identify the HMTs responsible for H3K4me3 at *LAMC2* and *CYR61* promoters, we depleted these 6 HMTs in HCT116 cells (Supplemental Figure 6A). As shown in Figure 6A, depleting SETD1A, but not the other HMTs, decreased H3K4me3 at their promoters. Moreover, SETD1A had much more enrichment at their promoters than the other HMTs did (Supplemental Figure 6B). These results strongly suggest that SETD1A is responsible for H3K4me3 at the promoters of *LAMC2* and *CYR61*.

To test whether SETD1A is required for PHGDH K146mUb-promoted tumor cell migration, we overexpressed SETD1A WT

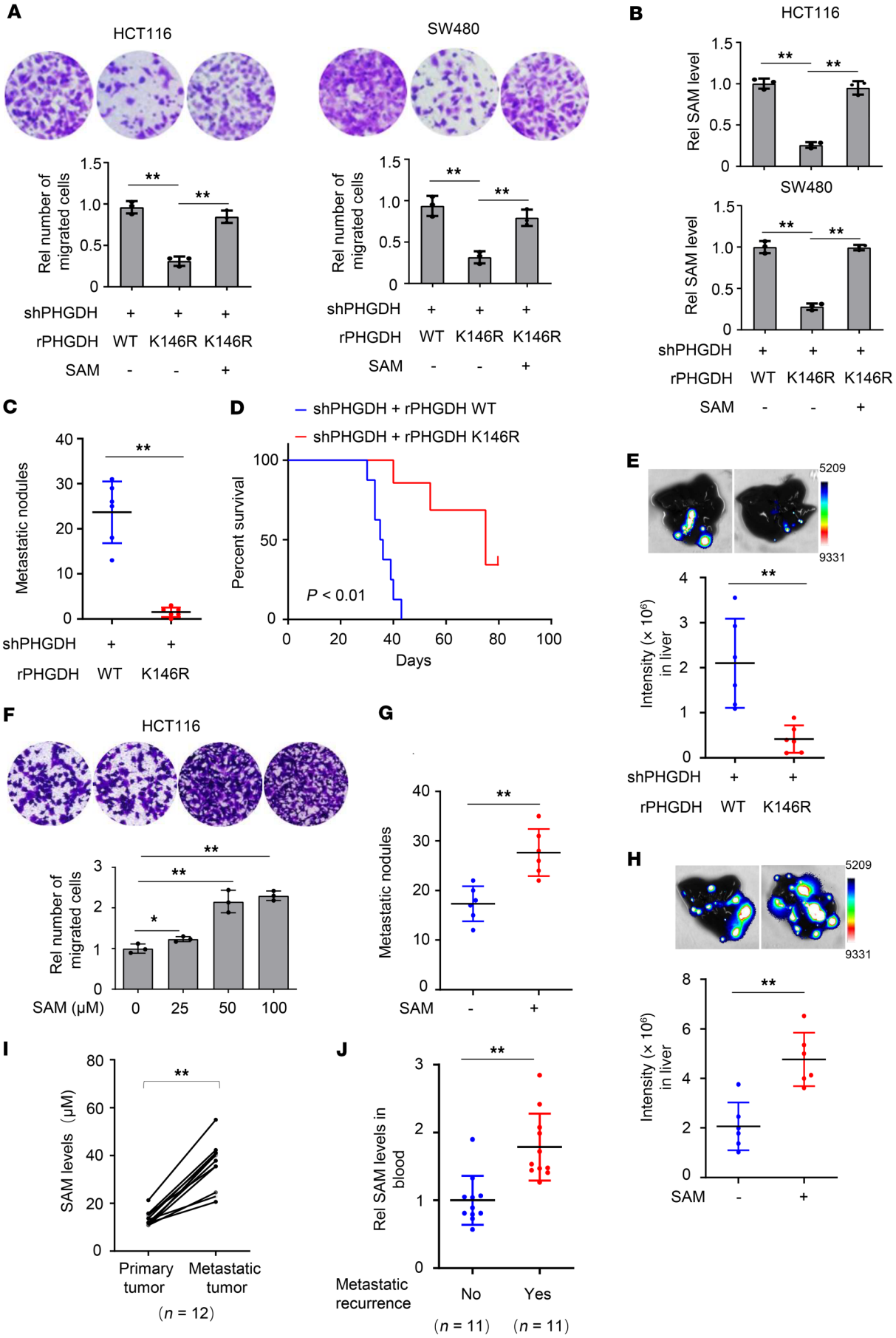
A
HCT116
SW480
Rel number of migrated cells
shPHGDH
rPHGDH WT K146R K146R
SAM
B
HCT116
SW480
Rel SAM level
C
Metastatic nodules
D
shPHGDH + rPHGDH WT
shPHGDH + rPHGDH K146R
Percent survival
P < 0.01
Days
E
5209
9331
Intensity (× 10⁶) in liver
F
HCT116
SAM (μM)
G
Metastatic nodules
H
I
SAM levels (μM)
Primary tumor
Metastatic tumor
(n = 12)
J
Rel SAM levels in blood
Metastatic recurrence
No
Yes
(n = 11)

Figure 4. Increased SAM levels by PHGDH K146mUb promote CRC metastasis. (**A**–**E**) PHGDH-depleted HCT116 or SW480 cells were rescued with rPHGDH WT or K146R. These cells were supplemented with or without SAM (25 μM). Transwell migration assays were performed (**A**). Intracellular SAM levels were examined (**B**). These cells were injected into spleens (**C** and **D**), or HCT116-derived tumors were implanted into cecum (**E**), of randomized BALB/c nude mice. The metastatic nodules in the livers were counted and statistically analyzed (**C**). Data represent the mean ± SD of 6 mice (2-tailed *t* test). Kaplan-Meier survival analysis was performed (**D**). Upward tick mark represents censored (alive) mice. Eight weeks after the implantation, bioluminescence imaging of the dissected livers was performed (**E**). Representative images of hepatic metastasis were shown (top). Data represent mean ± SD of luciferase intensities from 6 mice (bottom, 2-tailed *t* test). (**F**) Transwell migration assays were performed with HCT116 cells treated with increasing doses of SAM. (**A**, **B**, and **F**) Data represent the mean ± SD of 3 biologically independent experiments (1-way ANOVA with Tukey's multiple-comparison test). (**G** and **H**) HCT116 cells were injected into spleens (**G**), or HCT116-derived tumors were implanted into cecum (**H**), of randomized BALB/c nude mice, followed by SAM administration (20 mg/kg body weight). The metastatic nodules in dissected livers were counted and statistically analyzed (**G**). Data represent the mean ± SD of 6 mice (2-tailed *t* test). Bioluminescence imaging of the dissected liver tissues was performed (**H**). Representative images of hepatic metastasis were shown (top). Data represent mean ± SD of luciferase intensities from 6 mice (bottom, 2-tailed *t* test). (**I**) SAM levels were compared between primary tumors and paired metastatic tumors from 12 patients with CRC (paired *t* test, 2 tailed). (**J**) SAM levels in blood samples were compared between patients with CRC with or without metastatic recurrence. Data represent the mean ± SD (2-tailed *t* test). $^{*}P < 0.05$, $^{**}P < 0.01$. See also Supplemental Figure 4.

or catalytically inactive mutant (SETD1A$^{\Delta SET}$), in which SET domain (aa 1506–1707) was deleted in full-length SETD1A (16), in PHGDH-depleted HCT116 cells rescued with rPHGDH K146R. SETD1A WT, but not SETD1A$^{\Delta SET}$ overexpression, greatly recovered H3K4me3 at the promoters of *LAMC2* and *CYR61* (Figure 6B and Supplemental Figure 6C), suggesting that SETD1A is required for the histone methylation of these 2 genes through its methyltransferase activity. Consistently, SETD1A overexpression recovered the expressions of *LAMC2* and *CYR61* and the ability to migrate in tumor cells rescued with rPHGDH K146R (Figure 6, C and D, and Supplemental Figure 6D). Also, we depleted SETD1A in HCT116 cells and rescued with rSETD1A WT (Supplemental Figure 6E). As shown in Supplemental Figure 6F and Figure 6, E and F, SETD1A depletion inhibited the expressions of *LAMC2* and *CYR61* and tumor cell migration, while rescued expression of rSETD1A restored the expressions of those genes and cell migration in SETD1A-depleted tumor cells.

To investigate how PHGDH K146mUb specifically regulates SETD1A-mediated histone methylation, we first examined the recruitment of SETD1A to the promoters of *LAMC2* and *CYR61* genes, which showed that rescued expression of rPHGDH K146R did not influence SETD1A enrichment at the promoters (Supplemental Figure 6G). Given that PHGDH K146mUb increases SAM levels and that SETD1A requires SAM for histone methylation, we thought that PHGDH K146mUb might activate SETD1A by increasing SAM levels. To test this hypothesis, we determined the concentration of SAM that is required for the methylation reaction catalyzed by the H3K4me3 HMTs, such as KMT2A, KMT2C, KMT2D, SETD1A, SETD1B, or SMYD3. We purified the methyltransferase domains of these HMTs from *E. coli* (ref. 15 and Supplemental Figure 6H). In vitro methylation assay was performed by mixing these methyltransferase domains and histone H3K4 peptide with increasing amounts of SAM. Dot blot assay with anti-H3K4me3 antibody showed that SETD1A demanded higher levels of SAM for the methylation reaction, compared with the other HMTs (Figure 6G). Notably, SETD1A was almost fully activated in the presence of 50 μM SAM (Supplemental Figure 6I). Moreover, isothermal titration calorimetry (ITC) assay showed that SETD1A had the lowest affinity for SAM among these H3K4me3 HMTs (Figure 6H). These results indicate that because of low SAM affinity, SETD1A requires high levels of SAM for its activation. K146mUb enhances PHGDH activity and increases the levels of SAM, thereby activating SETD1A-mediated histone methylation, increasing cell adhesion gene expression and promoting CRC metastasis.

Discussion

Despite its role in primary tumors, deregulated metabolism is also important to the metastatic process, though which metabolic pathway is rewired, how it is rewired, and how the rewired pathway supports tumor metastasis remain poorly understood. Although metabolism and epigenetics are closely linked and play a crucial role in many aspects of cancer, how fluctuating levels of metabolite specifically regulate specific gene expression remains elusive. In this study, we demonstrate that Cul4A-DDB1–mediated monoubiquitination of PHGDH is important for tumor metastasis by regulating serine biosynthesis, 1-carbon metabolism, and epigenetics. Mechanistically, PHGDH K146mUb recruits DNAJA1 to facilitate the tetrameric formation of PHGDH, which increases PHGDH activity and downstream SAM levels. Increased levels of SAM specifically activate SETD1A, which catalyzes histone H3K4me3 and upregulates the expression of *LAMC2* and *CYR61* genes, thereby promoting tumor metastasis (Figure 7). These findings demonstrate a potentially new role and regulatory mechanism of PHGDH in tumor metastasis and provide insight into how fluctuating SAM levels regulate specific gene expression. Our study not only provides a link between metabolic status and cell migration but also uncovers a layer of the specificity of epigenetic regulation.

As the catalyst of the first committed step of serine biosynthesis, PHGDH is regulated by multiple mechanisms, including genomic amplification, transcription, and posttranslational modification. For example, PHGDH is recurrently amplified in a genomic region of focal copy number gain, most commonly found in melanoma and breast cancer (5, 17). P53 suppresses PHGDH expression and inhibits de novo serine biosynthesis in human melanoma cells (18). HOXA10 represses PHGDH expression to regulate the differentiation of human endometrial epithelium (19). PKC-ζ phosphorylates PHGDH to inhibit its enzymatic activity, thereby impairing tumorigenesis (6). In addition to phosphorylation, PHGDH is also polyubiquitinated by the E3 ligase Parkin at K330, which leads to PHGDH degradation and suppresses serine synthesis and cell proliferation (20). Deubiquitinating enzyme JOSD2 could also regulate the protein stability of PHGDH through an unknown mechanism, which might promote lung cancer growth (21). However, little is known about how PHGDH is regulated during tumor metastasis. In this study, we show that PHGDH is monoubiquitinated at K146 by Cul4A-DDB1

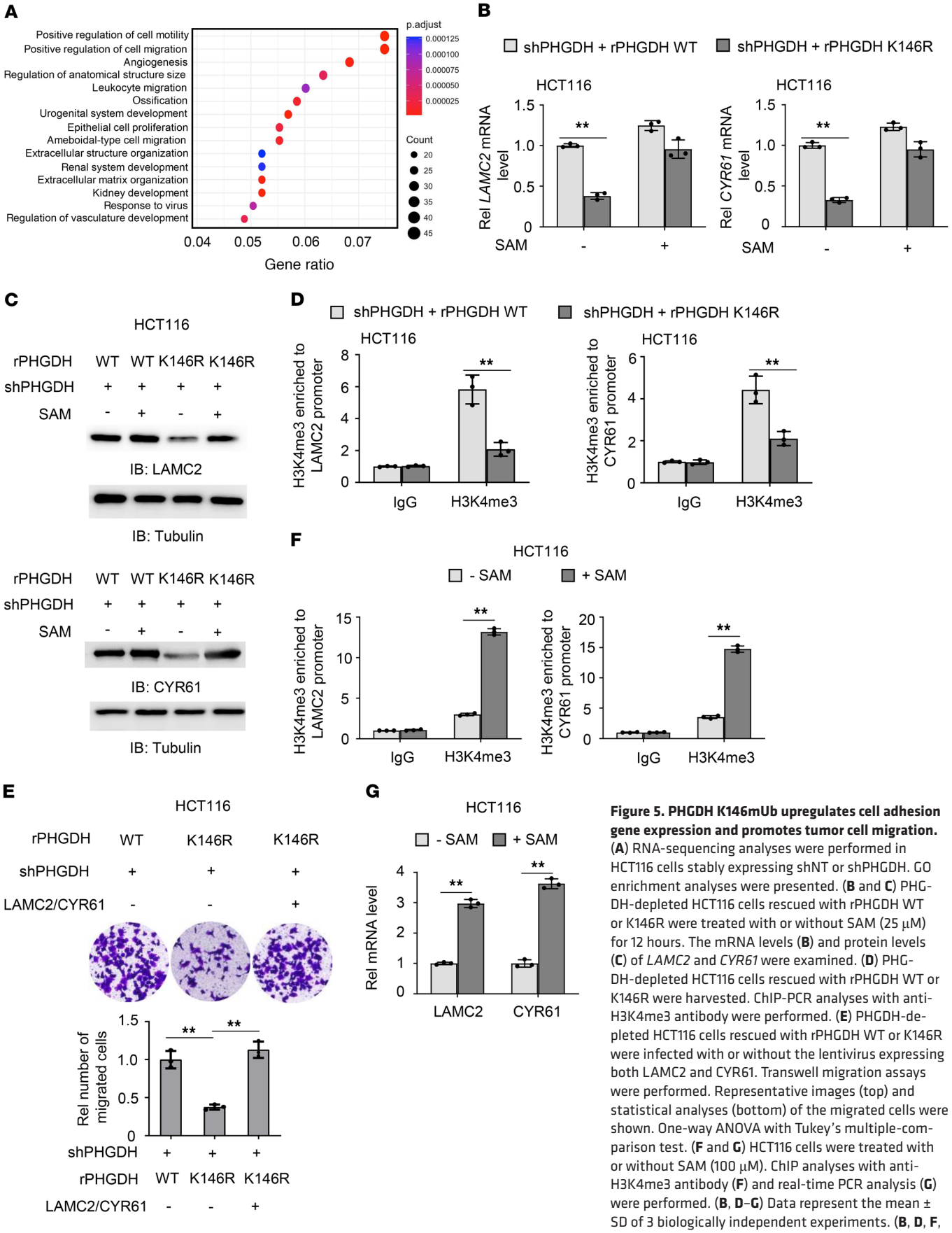

Figure 5. PHGDH K146mUb upregulates cell adhesion gene expression and promotes tumor cell migration. (**A**) RNA-sequencing analyses were performed in HCT116 cells stably expressing shNT or shPHGDH. GO enrichment analyses were presented. (**B** and **C**) PHGDH-depleted HCT116 cells rescued with rPHGDH WT or K146R were treated with or without SAM (25 μM) for 12 hours. The mRNA levels (**B**) and protein levels (**C**) of *LAMC2* and *CYR61* were examined. (**D**) PHGDH-depleted HCT116 cells rescued with rPHGDH WT or K146R were harvested. ChIP-PCR analyses with anti-H3K4me3 antibody were performed. (**E**) PHGDH-depleted HCT116 cells rescued with rPHGDH WT or K146R were infected with or without the lentivirus expressing both LAMC2 and CYR61. Transwell migration assays were performed. Representative images (top) and statistical analyses (bottom) of the migrated cells were shown. One-way ANOVA with Tukey's multiple-comparison test. (**F** and **G**) HCT116 cells were treated with or without SAM (100 μM). ChIP analyses with anti-H3K4me3 antibody (**F**) and real-time PCR analysis (**G**) were performed. (**B**, **D**–**G**) Data represent the mean ± SD of 3 biologically independent experiments. (**B**, **D**, **F**, and **G**) 2-tailed Student's *t* test. $^{**}P < 0.01$. See also Supplemental Figure 5.

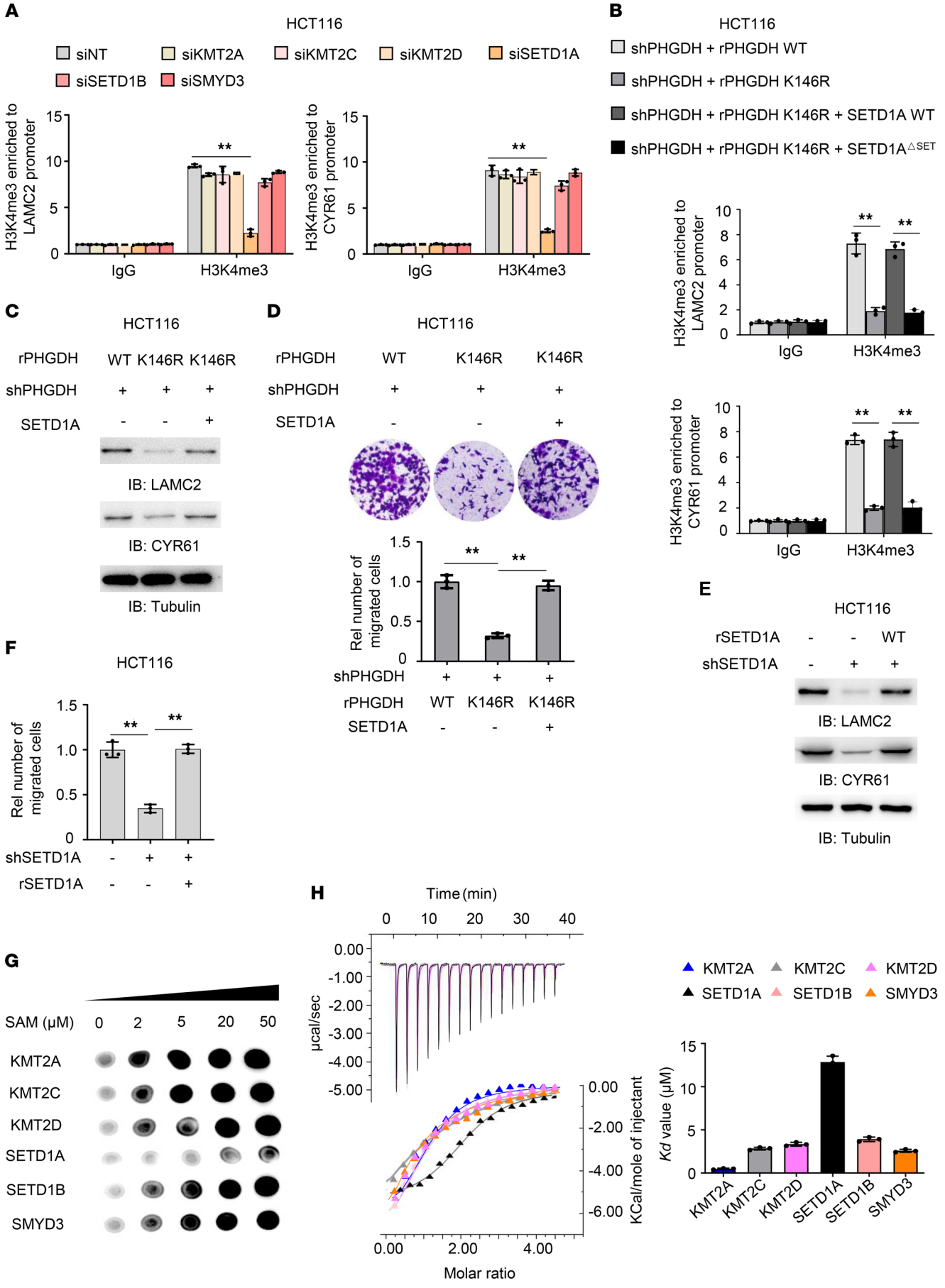
A
HCT116
siNT
siKMT2A
siKMT2C
siKMT2D
siSETD1A
siSETD1B
siSMYD3
H3K4me3 enriched to LAMC2 promoter
H3K4me3 enriched to CYR61 promoter
IgG
H3K4me3
B
HCT116
shPHGDH + rPHGDH WT
shPHGDH + rPHGDH K146R
shPHGDH + rPHGDH K146R + SETD1A WT
shPHGDH + rPHGDH K146R + SETD1A△SET
C
HCT116
rPHGDH WT K146R K146R
shPHGDH + + +
SETD1A - - +
IB: LAMC2
IB: CYR61
IB: Tubulin
D
HCT116
rPHGDH WT K146R K146R
shPHGDH + + +
SETD1A - - +
Rel number of migrated cells
E
HCT116
rSETD1A - - WT
shSETD1A - + +
IB: LAMC2
IB: CYR61
IB: Tubulin
F
HCT116
Rel number of migrated cells
shSETD1A - + +
rSETD1A - - +
G
SAM (μM) 0 2 5 20 50
KMT2A
KMT2C
KMT2D
SETD1A
SETD1B
SMYD3
H
Time (min)
μcal/sec
KCal/mole of injectant
Molar ratio
KMT2A KMT2C KMT2D
SETD1A SETD1B SMYD3
Kd value (μM)

Figure 6. Increased SAM levels by PHGDH K146mUb promote tumor cell migration by initiating SETD1A-mediated histone methylation of *LAMC2* and *CYR61*. (**A**) HCT116 cells were transfected with siRNAs targeting nontargeting (NT), KMT2A, KMT2C, KMT2D, SETD1A, SETD1B, or SMYD3. ChIP analyses with anti-H3K4me3 antibody were performed. (**B**) PHGDH-depleted HCT116 cells rescued with rPHGDH WT or K146R were infected with or without the lentivirus expressing SETD1A or SETD1A$^{\Delta SET}$. ChIP analyses were performed with anti-H3K4me3 antibody. (**C** and **D**) PHGDH-depleted HCT116 cells rescued with rPHGDH WT or K146R were infected with or without the lentivirus expressing SETD1A. Immunoblotting analyses were performed (**C**). Transwell migration assays were performed (**D**). (**E** and **F**) HCT116 cells were depleted of endogenous SETD1A and rescued with rSETD1A. LAMC2 and CYR61 expression was examined by immunoblotting analyses (**E**). Transwell migration assay was performed in these cells (**F**). (**G**) In vitro methylation assays were performed with purified recombinant His-tagged methyltransferase domains of KMT2A, KMT2C, KMT2D, SETD1A, SETD1B or SMYD3, SAM, and H3K4 peptide, followed by dot blot analysis with anti-H3K4me3 antibody. (**H**) ITC assays were performed with purified recombinant His-tagged methyltransferase domains of indicated HMTs and SAM. Representative images (left) and statistical results (right) of ITC were shown. (**A**, **B**, **D**, **F**, and **H**) Data represent the mean ± SD of 3 biologically independent experiments. One-way ANOVA with Tukey's multiple-comparison test. $^{**}P < 0.01$. See also Supplemental Figure 6.

E3 ligase complex. This K146 monoubiquitination recruits a chaperone protein, DNAJA1, to facilitate PHGDH tetrameric formation, thereby enhancing its activity. Our finding demonstrates a potentially new regulatory mechanism of PHGDH activity by monoubiquitination during tumor metastasis and suggests a therapeutic strategy by inhibiting PHGDH monoubiquitination to treat CRC metastasis.

As reported previously, a PHGDH inhibitor constrains tumor growth in a xenograft mouse model of CRC (22, 23). In contrast, our finding demonstrates that, in a PDX mouse model of CRC, a PHGDH inhibitor not only inhibits tumor growth but also inhibits tumor metastasis, suggesting the therapeutic potential of a PHGDH inhibitor in blocking tumor growth and metastasis.

SAM is the regulator of a variety of processes, including polyamine biosynthesis; amino acid metabolism; and DNA, RNA, and histone methylation. Maintenance of proper levels of the methyl donor SAM is critical for a wide variety of biological processes. In mouse models, excess levels of SAM have been implicated in erroneous methylation patterns associated with diabetic neuropathy (24). Low SAM levels regulate *Caenorhabditis elegans* immune responses by restricting histone H3 methylation at *Pseudomonas*-responsive promoters and limiting their expression (25). Moreover, cancer cell proliferation is dependent on low levels of DNA methylation. In vitro supplementation of SAM has been shown to remethylate promoter sequences and decrease the expression of proto-oncogenes (26). However, whether and how SAM levels are deregulated in tumor metastasis and how deregulated SAM levels promote tumor metastasis remain largely unknown. In the present study, we demonstrate that PHGDH is monoubiquitinated in metastatic CRC cells, which enhances its activity and increases its downstream intermediate SAM levels. High levels of SAM increase the expression of cell adhesion genes *LAMC2* and *CYR61*, by specifically initiating SETD1A-mediated histone H3K4me3, thereby promoting the metastasis of CRC cells. Intriguingly, the administration of SAM via oral gavage sufficiently enhanced hepatic metastasis of CRC cells in mice. This finding defines a role of increased SAM levels to promote CRC metastasis and provides a link between metabolic status and cell migration. In addition, we define the clinical relevance of SAM levels. The metastatic tumors from patients with CRC had much higher levels of SAM than the paired primary tumors. Furthermore, high levels of SAM were associated with higher rates of metastatic recurrence of patients with CRC. These data implicate the prognostic and therapeutic potential of SAM in CRC metastasis.

Although more and more connections have been recently uncovered between metabolism and epigenetics, little is known about how fluctuating levels of metabolites, such as SAM and acetyl-CoA, regulate the expression of specific genes. In the present study, we explored how high levels of SAM specifically increase the expression of *LAMC2* and *CYR61*. We identified that SETD1A is required for high levels of SAM-increased H3K4me3 at these 2 genes' promoters. Intriguingly, high levels of SAM did not influence the recruitment of SETD1A to their promoters. We thus speculated that the activation of SETD1A requires high SAM levels. Indeed, compared with other H3K4me3 HMTs, SETD1A-catalyzed methylation reaction required higher levels of SAM, due to low SAM affinity of SETD1A, as determined by ITC assay. Collectively, these results demonstrate that high levels of SAM specifically activate SETD1A that resides in *LAMC2* and *CYR61* promoters to increase their expression. This finding uncovers a layer of the specificity of epigenetic regulation, in addition to transcription factor–guided recruitment of HMTs. The fluctuation of SAM levels leads to the activation of the HMTs with different SAM affinity to catalyze histone methylation and promote gene expression.

Methods

Materials

Antibodies. Rabbit polyclonal antibodies recognizing PHGDH (catalog PA5-27578), CYR61 (catalog PA5-78022), KMT2D (catalog PA5-49581), PSAT1 (catalog PA5-22124), and Uba1 (catalog PA5-17274) and mouse monoclonal antibodies recognizing HSP70 (catalog MA3-008) and LAMC2 (catalog MA5-24646) were purchased from Thermo Fisher Scientific. Mouse monoclonal antibodies against Actin (catalog 60008-1-lg) and DDB1 (catalog 66010-1-lg) and rabbit polyclonal antibodies against PHGDH (catalog 14719-1-AP) and DNAJA1 (catalog 11713-1-AP) were obtained from Proteintech Group. Mouse monoclonal antibody against Flag (catalog F3165) and anti-Flag M2 affinity gel (catalog A2220) were purchased from MilliporeSigma. Rabbit monoclonal antibodies against HA Tag (catalog 3724), KMT2C (catalog 53641), and SMYD3 (catalog 12859) were obtained from Cell Signaling Technology. IgG (catalog sc-2025) and mouse monoclonal antibodies recognizing Tubulin (catalog sc-5286) and ubiquitin (catalog sc-8017) were purchased from Santa Cruz Biotechnology. Rabbit polyclonal antibodies recognizing KMT2A (catalog NB600-256), SETD1A (catalog NB100-558), SETD1B (catalog NBP1-28684), UbcH6 (catalog NBP1-78983B), and DCAF16 (catalog NBP2-82812) were purchased from Novus Biologicals, Bio-Techne. Rabbit polyclonal antibodies against H3K4me3 (catalog 07-473) and H3K9ac (catalog 07-352) were obtained from MilliporeSigma. Rabbit monoclonal antibody recognizing Cul4A (catalog A5064) was obtained from ABclonal Technology.

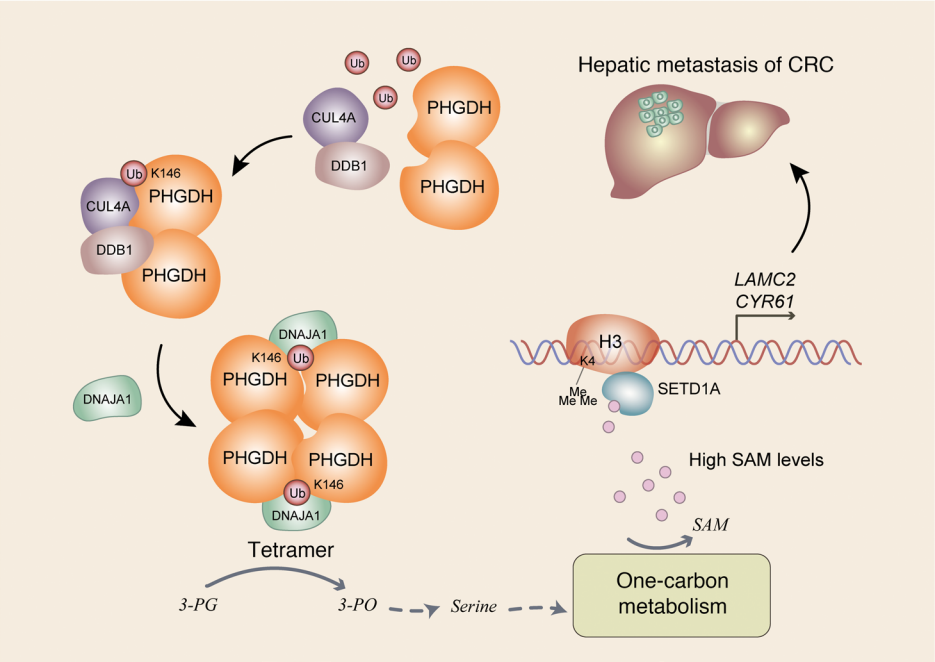

Figure 7. Schematic model of PHGDH monoubiquitination–promoted CRC metastasis. Cul4A-DDB1–mediated K146 monoubiquitination of PHGDH recruits DNAJA1 to facilitate tetrameric formation of PHGDH, which enhances its enzymatic activity and increases SAM levels. Increased levels of SAM specifically initiate SETD1A-mediated histone H3K4me3 to upregulate *LAMC2* and *CYR61* expression, thereby promoting tumor cell migration and CRC metastasis. 3-PG, 3-phosphoglycerate; 3-PO, 3-phosphooxypyruvate.

Reagents. Flag peptide and H3K4 peptide were obtained from ABclonal Technology. PHGDH inhibitor NCT-503, SAM, and SAH were purchased from MilliporeSigma. Serine Assay Kit, Glycine Assay Kit, and SAM ELISA Kit were brought from BioVision. Puromycin and hygromycin were bought from EMD Biosciences. In vitro DNA transfection reagent was purchased from SignaGen Laboratories. GelCode Blue Stain Reagent was obtained from Pierce, Thermo Fisher Scientific.

DNA constructs and mutagenesis

PCR-amplified human PHGDH; Cul4A; DNAJA1; DCAF16; LAMC2; CYR61; ubiquitin; Uba1; UbcH6; SETD1A; and methyltransferase domain of KMT2A, KMT2C, KMT2D, SETD1A, SETD1B, and SMYD3 were subcloned into pCDH, pCDH-SFB, pCDH-Flag, pcDH-HA, pcDNA6.0-V5-HIS, pGEX-GST, or pET-28a vectors. PHGDH, DNAJA1, and SETD1A mutations were constructed using the QuikChange Site-Directed Mutagenesis Kit (Stratagene, Agilent Technologies).

pGIPZ shNT was generated with the control oligonucleotide 5′-GCTTCTAACACCGGAGGTCTT-3′. pGIPZ PHGDH shRNA was generated with 5′-CACGACAGGCTTGCTGAATGA-3′ oligonucleotide. pGIPZ DNAJA1 shRNA was generated with 5′-ATATGGTCTACGATAAATTGG-3′ oligonucleotide. pGIPZ SETD1A shRNA was generated with 5′-GTTACCTTGAATGAAGGCAGA-3′ oligonucleotide. pGIPZ LAMC2 shRNA was generated with 5′-TATAGTAACCTGATCGACACC -3′ oligonucleotide. pGIPZ CYR61 shRNA was generated with 5′- TTGAACAGCCTGTAGAAGGGA-3′ oligonucleotide.

siRNA and transfection

siNC sequence is 5′-UUCUCCGAACGUGUCACGU-3′; Cul4A siRNA sequence is 5′-AAGAACUGAUCGCAAAGCAU-3′; DDB1 siRNA sequence is 5′-UAACAUGAGAACUCUUGUC-3′; KMT2A siRNA sequence is 5′-CUCUCCUCUCAAGUCUAAGUU-3′; KMT2C siRNA sequence is 5′-UGGUGUCAAAAAGAGAAAAAG-3′; KMT2D siRNA sequence is 5′-UCAAUGAGCACCUGAGGCUGG-3′; SETD1A siRNA sequence is 5′-GUUUGAACAGAUGACCAUCCU-3′; SETD1B siRNA sequence is 5′-AUGUGAAGGUGGAAUCAGAGA-3′; SMYD3 siRNA sequence is 5′-AGUAUCUCUUUGCUCAAUCAA-3′; PSAT1 siRNA sequence is 5′-AGAAGCCAAGAAGTTTGGGACTATA-3′; HSP70 siRNA sequence is 5′-GAAGCTTCCTGAAATGGACATTGAT-3′; and DCAF16 siRNA sequence is 5′-CCTCAGTAACCTACTGCCAGCTGAA-3′. siRNAs were synthesized by GenePharma. siRNAs were transfected using Lipofectamine RNAiMAX (Invitrogen, Thermo Fisher Scientific) according to the manufacturer's instructions and harvested 48 hours after transfection.

Cell culture

HEK293T cell line and the human colon adenocarcinoma cell lines HCT116 and SW480 were obtained from the Type Culture Collection of the Chinese Academy of Sciences. Cells were maintained in DMEM supplemented with 10% FBS and antibiotics. Cells were incubated in 5% CO_2 at 37°C. All cell lines were authenticated using the short tandem repeat method and tested negative for mycoplasma.

Immunoprecipitation and immunoblotting analysis

Extraction of proteins with a modified buffer from cultured cells was followed by immunoprecipitation and immunoblotting with corresponding antibodies, as described previously (27).

Cell proliferation assay

In brief, 2×10^4 cells in DMEM with 10% FBS were seeded per well in 6-well plates. Cells were counted with a Thermo Fisher Scientific Countess II FL.

PHGDH activity measurement

PHGDH activity was measured in 96-well plates at 25°C by monitoring NADH production. The change in absorbance at 340 nm was mea-

sured using BioTek Synergy Neo Multi-Mode Plate Reader (BioTek). Hydrazine hydrate was included to prevent product inhibition of PHGDH. Assays were performed in PHGDH reaction buffer (333 mM Tris-HCl pH 9.0, 1.67 mM EDTA, 7.23 mM 3-PG, 0.97 mM β-NAD, 3.27 mM glutathione). PHGDH was added to start the reaction.

Glycine and serine assays

Cells were collected for measurement of glycine and serine content using Glycine Assay Kit (BioVision) and Serine Assay Kit (BioVision).

SAM assay

SAM assay was performed using SAM ELISA Kit (BioVision), according to manufacturer instructions.

Purification of recombinant proteins

Recombinant methyltransferase domain of KMT2A, KMT2C, KMT2D, SETD1A, SETD1B, and SMYD3 and recombinant His-Ub, His-Uba1, His-UbcH6, and GST-PHGDH were expressed in bacteria and purified as described previously. Briefly, the vectors expressing methyltransferases were used to transform BL21/DE3 *E. coli* bacteria. Protein expression was induced in the presence of 0.5 mM Isopropyl-β-D-thiogalactopyranoside for 24 hours at 16°C. Cell pellets were collected and sonicated in PBS with the addition of proteasome inhibitors before centrifugation at 16,900*g* for 30 minutes (4°C). Cleared lysates were then bound to Ni-NTA resin (GenScript) or glutathione resin (GenScript) for 4 hours, with rolling at 4°C. Beads were washed extensively before eluting for 1 hour in His elution buffer (PBS plus 500 mM imidazole, pH 7.4) or GST elution buffer (50 mM Tris-HCl, 150 mM NaCl, 10 mg/mL glutathione, pH 8.0). Eluted proteins were then dialyzed against 40 mM Tris-HCl pH 7.4, 50 mM KCl, and 10 mM $MgCl_2$.

Isothermal calorimetric titration assay

ITC assay was performed by using a MicroCal VP-ITC type microcalorimeter (MicroCal Inc., Malvern Panalytical). Briefly, temperature equilibration was allowed for 1–2 hours until 25°C prior to the experiment. Purified proteins were dialyzed against 40 mM Tris-HCl (pH 7.4), 50 mM KCl, and 10 mM $MgCl_2$. SAM was diluted in 40 mM Tris-HCl (pH 7.4), 50 mM KCl, and 10 mM $MgCl_2$. All solutions were thoroughly degassed before being used by centrifugation at 16,900*g*, 4°C, for 10 minutes. The experiment was conducted by consecutively injecting small molecular solution into the calorimetric cell containing purified proteins. The titration enthalpy data were corrected for the small heat changes in control titrations of small molecular solution into the dialysis buffer.

Gel filtration

The gel filtration experiment was done as described previously (28).

Quantitative real-time reverse transcription PCR

Total cellular RNA was isolated with TRIzol (Invitrogen, Thermo Fisher Scientific) and reverse-transcribed into cDNA as described previously (29). Real-time PCR was performed on an Applied Biosystems 7500 using SYBR Green PCR Master mix (Thermo Fisher Scientific). Primer sequences used for the amplification of human *LAMC2* were 5′-CAAAGGTTCTCTTAGTGCTCGAT-3′ (forward) and 5′-CACTTGGAGTCTAGCAGTCTCT-3′ (reverse). Primer sequences used for the amplification of human *CYR61* were 5′-ACCGCTCTGAAGGGGATCT-3′ (forward) and 5′-ACTGATGTTTACAGTTGGGCTG-3′ (reverse).

ChIP assay

ChIP was performed with indicated antibodies using Simple ChIP Enzymatic Chromatin IP Kit (Cell Signaling Technology) according to manufacturer instructions. Primer sequences used for the amplification of human *LAMC2* promoter associated with H3K4me3, H3K9ac, or HMTs were 5′-ACTGTGCTAGTAGATAACATT-3′ (forward) and 5′-GATTATAGGCATAAACACCAT-3′ (reverse). Primer sequences used for the amplification of human *CYR61* promoter associated with H3K4me3 or HMTs were 5′-GAAGTCCACAAATATTCCTGA-3′ (forward) and 5′-AGTTCAGAACTTTGCCTGGAC-3′ (reverse).

Transwell migration assay

HCT116 or SW480 (1×10^5) cells were seeded into the upper chamber of a Transwell filter with 8 μm pores (Falcon, Corning) with serum-free medium. After 12 hours, cells were fixed with 4% paraformaldehyde in PBS. Nonmigrated cells on the upper side of the filter were removed with a cotton swab, and cells on the underside of the filter were stained with 0.4% crystal violet (Sangon Biotech) in 10% ethanol. In parallel, cells were separately plated into plates without Transwell filters to determine the total number of attached cells. The relative cell migration was calculated by the number of migrated cells normalized to the total number of cells, followed by further normalization to the control group. For each experiment, the number of cells in 5 random fields (magnification, 100×) on the underside of the filter was counted, and 3 independent filters were analyzed.

Mass spectrometry analyses

SFB-PHGDH proteins were immunoprecipitated from HCT116 cells. The precipitated complexes were boiled at 95°C for 10 minutes. SFB-PHGDH (for detection of PHGDH ubiquitination) and PHGDH-associated proteins were separated from the complexes using SDS-PAGE. The 2 fractions were processed as described previously (30), including reductive alkylation, trypsin digestion, and peptide extraction. The peptides were analyzed by liquid chromatography–tandem mass spectrometry on a Q Exactive mass spectrometer (Thermo Fisher Scientific).

Proteins were identified by a database search of the fragment spectra against the National SwissProt protein database (European Bioinformatics Institute) using Mascot Server 2.4 (Matrix Science). Ubiquitinated-peptide matches were analyzed using MaxQuant v.1.5.2.8 implemented in Proteome Discoverer (Thermo Fisher Scientific) and manually curated (31).

Intracellular metabolomics profiling

PHGDH-depleted HCT116 cells rescued with rPHGDH WT or K146R were harvested. An aqueous solution of 80%(v/v) methanol was used to extract intracellular metabolites. Extracted samples were analyzed with gas chromatography–mass spectrometry (GC-MS) metabolomics. The mixture was processed by 5 cycles of 1-minute ultrasonication with a 1-minute interval between cycles. The mixture was kept at –40°C for 24 hours prior to centrifugation at 16,000*g* at 4°C for 15 minutes. In total, 200 μL of supernatant and 10 μL internal standards (50 μg/mL L-norleucine and [6-^{13}C] glucose) were evaporated to dry-

ness under gentle nitrogen stream. The dry residue was reconstituted in 30 μL of 20 mg/mL methoxyamine hydrochloride in pyridine, and the resulting mixture was incubated at 37°C for 90 minutes. A total of 30 μL of *N,O*-bis(trimethylsily)trifluoroacetamide with 1% trimethylchlorosilane was added into the mixture and derivatized at 70°C for 60 minutes prior to GC-MS metabolomics analysis. Quality control samples pooled from cell samples in each group were prepared and analyzed with the same procedure as that for the experimental samples.

Metabolomics instrumental analysis was performed on an Agilent 7890A gas chromatography system coupled to an Agilent 5975C inert MSD system (Agilent Technologies). An Rxi-5 Sil MS fused-silica capillary column (30 m × 0.25 mm × 0.25 μm; Restek) was utilized to separate the derivatives. Helium (>99.999%) was used as a carrier gas at a constant flow rate of 1 mL/min through the column. Injection volume was 1 μL in split-less mode, and the solvent delay time was 6 minutes. The initial oven temperature was held at 70°C for 2 minutes; increased to 160°C at a rate of 6°C/min, to 240°C at a rate of 10°C/min, and to 300°C at a rate of 20°C/min; and finally held at 300°C for 6 minutes. The temperatures of injector, transfer line, and electron impact ion source were set to 250°C, 250°C, and 230°C, respectively. The impact energy was 70 eV, and data were collected in a full scan mode (*m/z* 50–600).

Quantification of targeted metabolomics was performed by applying MSD ChemStation (Version E.02.02.1431, Agilent Technologies) to observe the ion area (*m/z*).

In vitro ubiquitination assay

The in vitro ubiquitination assays were performed as described previously (32). HEK293T cells were transfected with Flag-Cul4A or HA-DCAF16. The Cul4A or DCAF16 proteins were immunoprecipitated and purified from the whole-cell lysates using anti–Flag-agarose (MilliporeSigma) or anti–HA-agarose beads (Aogma). Recombinant GST-PHGDH protein was incubated with purified Flag-Cul4A and HA-DCAF16 in the presence of recombinant active His-Uba1 (E1) and His-UbcH6 (E2), ATP, and His-ubiquitin. The reactions were stopped by the addition of 4× SDS-PAGE sample buffer, and the reaction products were resolved by SDS-PAGE gel and probed with the indicated antibodies.

IHC

The tissue sections from paraffin-embedded human lung tumors were stained with antibodies as indicated. We quantitatively scored the tissue sections according to the percentage of positive cells and staining intensity. We rated the intensity of staining on a scale of 0 to 3: 0, negative; 1, weak; 2, moderate; 3, strong. We assigned the following proportion scores: X indicates the percentage of the tumor cells that were stained ($0 \le [X1 + X2 + X3] \le 100$), where X1 indicates weak staining, X2 moderate staining, and X3 strong staining. The score (H score) was obtained using the formula: $1 \times X1 + 2 \times X2 + 3 \times X3$, giving a range of 0 to 300.

Subcutaneous xenograft model

In brief, 2×10^6 HCT116 cells were subcutaneously injected into the left dorsal part of randomized 6-week-old female BALB/c nude mice purchased from SLAC Laboratory Animal Co., Ltd. (6 mice per group). After inoculation for 20 days, mice were euthanized and tumors were dissected.

Mouse model of hepatic metastasis of CRC

In brief, 5-week-old female BALB/c nude mice were purchased from SLAC Laboratory Animal Co., Ltd. As described previously (33), 1×10^5 HCT116 cells were injected into mouse spleens. Six mice were included in each experiment. Four weeks after inoculation, mice were euthanized, and mouse livers were dissected and fixed in 4% paraformaldehyde. Livers were embedded by paraffin and subjected to H&E staining. For SAM treatment, 1 week after injection, these mice were administrated with SAM via oral gavage once daily for 3 weeks. Four weeks after the injection, mouse livers were dissected. The metastatic nodules in the livers were counted and statistically analyzed.

Orthotopic implantation was performed as described previously (34). Briefly, 2×10^6 luciferase-expressing HCT116 cells were inoculated subcutaneously into female BALB/c nude mice. Once xenografts were established, they were excised and minced into 1–2 mm^3 pieces. Orthotopic implantation procedure into other female BALB/c nude mice was performed using these pieces. For SAM treatment, 2 weeks after the implantation, these mice were administrated with SAM via oral gavage once daily for 4 weeks. Eight weeks after the injection, bioluminescence imaging of the dissected liver tissues from the mice was performed.

SAM was mixed in PBS and given daily at 20 mg/kg body weight in 100 μL via gavage.

All mice were maintained in pathogen-free facilities at the Shanghai Institute of Biochemistry and Cell Biology (SIBCB). Animals were randomly allocated to experimental groups. The animal experiments were performed in a blinded manner.

PDX model of CRC metastasis

Fresh tumor samples were obtained from patients at Fudan University Shanghai Cancer Center. Tumor tissues were immediately transferred on ice in a DMEM-based medium supplemented with 2% v/v penicillin/streptomycin. Tumor material was then dissected, cut into 60 mm^3 pieces, and quickly embedded into Matrigel prior to being grafted subcutaneously into the flanks of BALB/c nude mice. Once the xenograft reached 6 weeks, mice were operated on, and tumors were dissected, cut into small pieces (60 mm^3), and regrafted in a new generation of mice. One week after inoculation, mice were treated with NCT-503 for 3 weeks. Five weeks after inoculation, mice were euthanized, and mouse livers were dissected and fixed in 4% paraformaldehyde. Livers were embedded by paraffin and subjected to H&E staining.

For NCT-503 treatment, NCT-503 was prepared in a vehicle of 5% ethanol, 35% PEG 300 (MilliporeSigma), and 60% of an aqueous 30% hydroxypropyl-β-cyclodextrin (MilliporeSigma) solution and injected intraperitoneally once daily at 25 mg/kg body weight.

In vitro methylation assay

We purified recombinant His-tagged HMT domains of KMT2A, KMT2C, KMT2D, SETD1A, SETD1B, and SMYD3 from *E. coli*. In vitro HMT assay was performed as described previously (35). We adjusted the relative concentration of peptide and HMT in the reaction system: H3K4 peptide (ARTKQTARKSTG), 5 μM; His-tagged HMT domain, 200 nM.

Patient information

Age and sex were randomly distributed in different groups. Sample numbers are large enough for statistical analysis. Five cohorts

of patients with CRC were used in the study. IHC analyses of PHGDH were performed in tumor tissues and paired peritumoral tissues from 59 patients with CRC (Figure 1D); IHC analyses of PHGDH and immunoblotting analyses of PHGDH mUb were performed in 40 CRC patients without metastatic recurrence and 31 CRC patients with metastatic recurrence, all of whom received standard adjuvant radiotherapy and chemotherapy after surgery (Figure 1E and Supplemental Figure 2B); IHC analyses of PHGDH, Cul4A, or DDB1 were performed in paired primary and hepatic metastatic tumors from 10 CRC patients without previous treatment with radiotherapy or chemotherapy before surgery (Figure 1F, Figure 3H, and Supplemental Figure 3D); establishment of the PDX model of CRC metastasis and measurement of intracellular SAM concentrations were performed in paired primary and hepatic metastatic tumors from 12 CRC patients without previous treatment with radiotherapy or chemotherapy before surgery (Figure 1I; Figure 4I; Supplemental Figure 1, J and K; and Supplemental Figure 5C). Blood SAM concentrations were determined in 11 CRC patients with metastatic recurrence and 11 CRC patients without metastatic recurrence, all of whom received standard adjuvant radiotherapy and chemotherapy after surgery (Figure 4J).

Materials availability

This study did not generate new reagents.

Data and code availability

The RNA-sequencing data reported in this paper have been deposited in the National Center for Biotechnology Information's Gene Expression Omnibus (GEO) database. The accession number for the RNA-sequencing data reported in this paper is GEO GSE150261.

Statistics

No statistical methods were used to predetermine sample size. Wilcoxon's signed-rank test was used to analyze *PHGDH* mRNA levels between tumor tissues and paired normal tissues and among different stages of colon adenocarcinoma tissues (Figure 1, A and B). Kaplan-Meier method was used to analyze the statistical significance of the survival correlations between groups (Figure 1C and Figure 4D). A paired, 2-tailed Student's *t* test was used for 2-group comparisons (Figure 1, D and F; Figure 3H; Figure 4I; and Supplemental Figure 3D). Besides the 3 analyses mentioned above, an unpaired, 2-tailed Student's *t* test was used for 2-group comparisons, whereas 3 or more groups were compared using 1-way ANOVA followed by Tukey's multiple-comparison test. $P < 0.05$ was considered significant. $P < 0.01$ was considered extremely significant.

Study approval

The use of human CRC tissues and paired metastatic tumor tissues, CRC tissues, and blood samples of CRC patients with or without metastatic recurrence was approved by the institutional review board at Fudan University Shanghai Cancer Center and complied with all relevant ethical regulations. The use of human CRC tissues and paired peritumoral tissues was approved by the institutional review board at Changhai Hospital (Shanghai, China) and complied with all relevant ethical regulations. Written informed consent was obtained from all patients.

All animal experiments were approved by the IACUC of SIBCB, Chinese Academy of Sciences, and complied with all relevant ethical regulations.

Author contributions

This study was conceived by WY; WY, XW, and YZ designed the study; XW, YZ, HY, and JZ performed the experiments; YZ also contributed to data analyses and figure editing; SW and SL contributed to the schematic model and TCGA data analyses; HG, PW, and JL provided experiment assistance; GY, XL, and DL provided reagents and assistance with pathology; and WY wrote the manuscript with comments from all authors.

Acknowledgments

This work was supported by the National Natural Science Foundation of China (92053203 and 32025013) to WY; the National Key Research and Development Program of China (2019YFA0802000) to WY; Chinese Academy of Sciences (CAS) Interdisciplinary Innovation Team (JCTD-2018-14) to WY; CAS Project for Young Scientists in Basic Research (YSBR-014) to WY; Program of Shanghai Academic/Technology Research Leader (20XD1424400) to WY; CAS Facility-based Open Research Program to WY; the National Natural Science Foundation of China (81902807) to YZ; National Postdoctoral Program for Innovative Talents (BX20190349) to YZ; Shanghai Post-doctoral Excellence Program (2018244) to YZ; China Postdoctoral Science Foundation (2020M671258) to YZ; the National Natural Science Foundation of China (81772583 and 81972293) to DL; Shanghai Rising Star Program (17QA1400900) to DL; and Municipal Human Resources Development Program for Outstanding Young Talents in Medical and Health Sciences in Shanghai (2017YQ046) to DL. We thank Genome Tagging Project Center and all the core facilities of SIBCB for technical support.

Address correspondence to: Weiwei Yang, Shanghai Institute of Biochemistry and Cell Biology, Chinese Academy of Science, 320 Yueyang Road, Shanghai 200031, China. Phone: 86.21.54921295; Email: wyang@sibcb.ac.cn. Or to: Dawei Li, Fudan University Shanghai Cancer Center, 270 Dongan Road, Shanghai 200032, China. Phone: 86.21.64175590.81110; Email: li_dawei@fudan.edu.cn. Or to: Xinxiang Li, Fudan University Shanghai Cancer Center, 270 Dongan Road, Shanghai 200032, China. Phone: 86.21.64175590.81110; Email: lxx1149@163.com. Or to: Xiongjun Wang, Guangzhou University, 230 Huanxi Road, Guangzhou 511442, China. Phone: 86.20.86236055; Email: xjwang02@sibcb.ac.cn.

1. Torre LA, et al. Global cancer statistics, 2012. *CA Cancer J Clin*. 2015;65(2):87–108.
2. Siegel R, et al. Colorectal cancer statistics, 2014. *CA Cancer J Clin*. 2014;64(2):104–117.
3. Amelio I, et al. Serine and glycine metabolism in cancer. *Trends Biochem Sci*. 2014;39(4):191–198.
4. Locasale JW. Serine, glycine and one-carbon units: cancer metabolism in full circle. *Nat Rev Cancer*. 2013;13(8):572–583.
5. Possemato R, et al. Functional genomics reveal that the serine synthesis pathway is essential in breast cancer. *Nature*. 2011;476(7360):346–350.
6. Ma L, et al. Control of nutrient stress-induced metabolic reprogramming by PKCζ in tumorigenesis. *Cell*. 2013;152(3):599–611.
7. Samanta D, et al. PHGDH expression is required for mitochondrial redox homeostasis, breast

cancer stem cell maintenance, and lung metastasis. *Cancer Res*. 2016;76(15):4430–4442.
8. Chiang PK, et al. S-Adenosylmethionine and methylation. *FASEB J*. 1996;10(4):471–480.
9. Dey S, et al. Crystal structure of Mycobacterium tuberculosis D-3-phosphoglycerate dehydrogenase: extreme asymmetry in a tetramer of identical subunits. *J Biol Chem*. 2005;280(15):14892–14899.
10. Achouri Y, et al. Cloning, sequencing and expression of rat liver 3-phosphoglycerate dehydrogenase. *Biochem J*. 1997;323(pt 2):365–370.
11. Qiu XB, et al. The diversity of the DnaJ/Hsp40 family, the crucial partners for Hsp70 chaperones. *Cell Mol Life Sci*. 2006;63(22):2560–2570.
12. Moon YW, et al. LAMC2 enhances the metastatic potential of lung adenocarcinoma. *Cell Death Differ*. 2015;22(8):1341–1352.
13. Kireeva ML, et al. Cyr61, a product of a growth factor-inducible immediate-early gene, promotes cell proliferation, migration, and adhesion. *Mol Cell Biol*. 1996;16(4):1326–1334.
14. Barski A, et al. High-resolution profiling of histone methylations in the human genome. *Cell*. 2007;129(4):823–837.
15. Rao RC, Dou Y. Hijacked in cancer: the KMT2 (MLL) family of methyltransferases. *Nat Rev Cancer*. 2015;15(6):334–346.
16. Sze CC, et al. Histone H3K4 methylation-dependent and -independent functions of Set1A/COMPASS in embryonic stem cell self-renewal and differentiation. *Genes Dev*. 2017;31(17):1732–1737.
17. Locasale JW, et al. Phosphoglycerate dehydrogenase diverts glycolytic flux and contributes to oncogenesis. *Nat Genet*. 2011;43(9):869–874.
18. Ou Y, et al. p53 Protein-mediated regulation of phosphoglycerate dehydrogenase (PHGDH) is crucial for the apoptotic response upon serine starvation. *J Biol Chem*. 2015;290(1):457–466.
19. Du H, et al. 3-Phosphoglycerate dehydrogenase expression is regulated by HOXA10 in murine endometrium and human endometrial cells. *Reproduction*. 2010;139(1):237–245.
20. Liu J, et al. Parkin ubiquitinates phosphoglycerate dehydrogenase to suppress serine synthesis and tumor progression. *J Clin Invest*. 2020;130(6):3253–3269.
21. Zhang B, et al. PHGDH defines a metabolic subtype in lung adenocarcinomas with poor prognosis. *Cell Rep*. 2017;19(11):2289–2303.
22. Muthusamy T, et al. Serine restriction alters sphingolipid diversity to constrain tumour growth. *Nature*. 2020;586(7831):790–795.
23. Tajan M, et al. Serine synthesis pathway inhibition cooperates with dietary serine and glycine limitation for cancer therapy. *Nat Commun*. 2021;12(1):366.
24. Varela-Rey M, et al. S-adenosylmethionine levels regulate the schwann cell DNA methylome. *Neuron*. 2014;81(5):1024–1039.
25. Ding W, et al. s-adenosylmethionine levels govern innate immunity through distinct methylation-dependent pathways. *Cell Metab*. 2015;22(4):633–645.
26. Schmidt T, et al. Treatment of prostate cancer cells with S-adenosylmethionine leads to genome-wide alterations in transcription profiles. *Gene*. 2016;595(2):161–167.
27. Zhang Y, et al. Macrophage-associated PGK1 phosphorylation promotes aerobic glycolysis and tumorigenesis. *Mol Cell*. 2018;71(2):201–215.
28. Liu F, et al. PKM2 methylation by CARM1 activates aerobic glycolysis to promote tumorigenesis. *Nat Cell Biol*. 2017;19(11):1358–1370.
29. Zhang J, et al. Down-regulation of G9a triggers DNA damage response and inhibits colorectal cancer cells proliferation. *Oncotarget*. 2015;6:2917–2927.
30. Wang XJ, et al. Opposing roles of acetylation and phosphorylation in LIFR-dependent self-renewal growth signaling in mouse embryonic stem cells. *Cell Rep*. 2017;18(4):933–946.
31. Wu YB, et al. Concurrent quantification of proteome and phosphoproteome to reveal system-wide association of protein phosphorylation and gene expression. *Mol Cell Proteomics*. 2009;8(12):2809–2826.
32. Jin J, et al. Identification of substrates for F-box proteins. *Methods Enzymol*. 2005;399:287–309.
33. Ordonez-Moran P, et al. HOXA5 counteracts stem cell traits by inhibiting wnt signaling in colorectal cancer. *Cancer Cell*. 2015;28(6):815–829.
34. Rajput A, et al. Establishment and validation of an orthotopic metastatic mouse model of colorectal cancer. *ISRN Hepatol*. 2013;2013:206875.
35. Fingerman IM, et al. In vitro histone methyltransferase assay. *CSH Protoc*. 2008; http://doi.org/10.1101/pdb.prot4939.